PULSE PHASE RESOLVED X-RAY SPECTROSCOPY OF FOUR ACCRETION POWERED MILLISECOND PULSARS

A THESIS SUBMITTED TO
THE GRADUATE SCHOOL OF NATURAL AND APPLIED SCIENCES
OF
MIDDLE EAST TECHNICAL UNIVERSITY

BY

SIDIKA MERVE ÇOLAK

IN PARTIAL FULFILLMENT OF THE REQUIREMENTS
FOR
THE DEGREE OF MASTER OF SCIENCE
IN
PHYSICS

AUGUST 2014

Approval of the thesis:

PULSE PHASE RESOLVED X-RAY SPECTROSCOPY OF FOUR ACCRETION POWERED MILLISECOND PULSARS

submitted by **SIDIKA MERVE ÇOLAK** in partial fulfillment of the requirements for the degree of **Master of Science in Physics Department, Middle East Technical University** by,

Prof. Dr. Canan Özgen _____
Dean, Graduate School of **Natural and Applied Sciences**

Prof. Dr. Mehmet Zeyrek _____
Head of Department, **Physics**

Prof. Dr. Altan Baykal _____
Supervisor, **Physics Dept., METU**

Examining Committee Members:

Prof. Dr. Ümit Kızıloğlu
Physics Dept., METU _____

Prof. Dr. Altan Baykal
Physics Dept., METU _____

Prof. Dr. Sacit Özdemir
Astronomy and Space Science Dept., Ankara University _____

Assoc. Prof. Dr. Sinan Kaan Yerli
Physics Dept., METU _____

Assoc. Prof. Dr. S. Çağdaş İnam
Electrical and Electronics Eng. Dept., Baskent University _____

Date: _____

I hereby declare that all information in this document has been obtained and presented in accordance with academic rules and ethical conduct. I also declare that, as required by these rules and conduct, I have fully cited and referenced all material and results that are not original to this work.

Name, Last Name: SIDIKA MERVE ÇOLAK

Signature :

ABSTRACT

PULSE PHASE RESOLVED X-RAY SPECTROSCOPY OF FOUR ACCRETION POWERED MILLISECOND PULSARS

Çolak, Sıdıka Merve

M.S., Department of Physics

Supervisor : Prof. Dr. Altan Baykal

August 2014, 65 pages

In this thesis, pulse phase resolved X-ray spectroscopy of four accretion powered millisecond pulsars which are IGR J00291+5934 , IGR J17498-2921 , XTE J0929-314 and XTE J1807-294 will be presented. Phase dependent changes during their outbursts will be checked for possible correlations of spectral parameters such as photon index and blackbody temperature with rotation phase using archive of Rossi X-ray Timing Explorer (RXTE) observations.

In the analysis of IGR J17498-2921 in 2011 outburst , positive correlation is found between photon index and flux. In the analysis of XTE J0929-314 in 2002 outburst, negative correlation is found between photon index and blackbody temperature. In the analysis of XTE J1807-294 in 2003 outburst, about 150 days RXTE observation data is divided into 7 states, which consist of 3 flare and 4 non-flare states. In the first flare state analysis, negative correlation is found between blackbody temperature and photon index. In the second flare state analysis, positive correlation is found between blackbody temperature and photon index. In the second non-flare state analysis, positive correlation is found between flux and photon index. In the fourth non-flare state analysis, positive correlation is found between flux and photon index. On the other hand, correlation between blackbody temperature, photon index and flux is not found in the analysis of third flare state, first non-flare state and third non-flare state analysis of XTE J1807-294 and in the analysis of IGR J00291+5934 in September 2008

outburst.

Keywords: Accreting Millisecond Pulsars, Phase-resolved X-ray Spectroscopy, RXTE, XTE J0929-314, IGR J00291+5934, IGR J17498-2921, XTE J1807-294

ÖZ

DÖRT KÜTLE AKTARIMI YAPAN MİLİSANİYE ATARCASININ PULS FAZ ÇÖZÜMLÜ X-IŞIN TAYF ÖLÇÜMÜ

Çolak, Sıdıka Merve
Yüksek Lisans, Fizik Bölümü
Tez Yöneticisi : Prof. Dr. Altan Baykal

Ağustos 2014 , 65 sayfa

Bu tezde, kütle aktarımlı milisaniye atarcası olan IGR J00291+5934 , IGR J17498-2921 , XTE J0929-314 ve XTE J1807-294 cisimlerinin faz çözümlü x-ışın tayfölçümü sunulmaktadır. Rossi X-ray Timing Explorer (RXTE) arşiv gözlemleri kullanılarak, cisimlerin patlamaları süresince faza bağlı değişiklikleri kontrol edilip, foton indisi ile karacisim sıcaklığı gibi tayfsal parametrelerdeki olası korelasyonlara bakılmaktadır.

IGR J17498-2921 cisminin 2011 patlamasının analizlerinde , foton indisi ile cismin akı değişimi parametreleri arasında pozitif korelasyon bulunmuştur. XTE J0929-314 cisminin 2002 patlamasının analizlerinde, karacisim sıcaklığı ile foton indisi arasında negatif korelasyon bulunmuştur. XTE J1807-294 cisminin 2003 patlaması analizlerinde, yaklaşık 150 günlük RXTE gözlem datası 3 patlama olan ve 4 patlama olmayan bölüm olmak üzere toplamda 7 bölüme ayrılmıştır. Birinci patlama bölümü analizlerinde , sıcaklığı ile foton indisi arasında negatif korelasyon bulunmuştur. İkinci patlama bölümü analizlerinde, karacisim sıcaklığı ile foton indisi arasında pozitif korelasyon bulunmuştur. İkinci patlama olmayan bölüm analizlerinde, foton indisi ile cismin akı değişimi parametreleri arasında pozitif korelasyon bulunmuştur. Dördüncü patlama olmayan bölüm analizlerinde foton indisi ile cismin akı değişimi parametreleri arasında pozitif korelasyon bulunmuştur. Öte yandan, XTE J1807-294 cisminin üçüncü patlama bölümü, birinci patlama olmayan bölümü ve üçüncü patlama olma-

yan bölümü analizleri ile IGR J00291+5934 cisminin 2008 Eylül patlaması analizlerinde karacisim sıcaklığı, foton indisi ve cismin akı değişimi parametreleri arasında net bir değişiklik bulunmamıştır.

Anahtar Kelimeler: Kütle Aktarımlı Milisaniye Atarcaları, Faz-çözümlü X-ışın Tayfölçümü, RXTE, XTE J0929-314, IGR J00291+5934, IGR J17498-2921, XTE J1807-294

This thesis is dedicated to the memory of my mother, Serpil Çolak, who taught me to question and imagine.

ACKNOWLEDGMENTS

Foremost, I would like to express my gratitude to my MSc advisor Altan Baykal for his invaluable guidance and supervision of my thesis. my advisor, I also wish to thank S. Çağdaş İnam for his contribution to the analysis with his relevant comments and detailed feedback on my thesis. I would also like to thank to M. Miraç Serim for inspiring me to learn and to start the analysis and to Mehtap Özbey Arabacıoğlu for her motivation on astrophysics and for her friendship as well. Special thanks goes Sinan Kaan Yerli who adviced me to see the broad picture of astrophysics and for his precious contributions to the format of the thesis. I am grateful to Ümit Kızıloğlu who taught me my first astrophysical analysis and to Şölen Balman for answering all of my observational and theoretical astrophysical questions. I would like to thank Nilgün Kızıloğlu who gave me my first astrophysics lessons in undergraduate and Halil Kirbiyik who encouraged me to pursue astrophysics. I would also like to thank to Emrah Kalemci for broadening my horizon by making it possible for me to attend astrophysics conferences and to Ali Alpar for his precious suggestions and his contributions to millisecond pulsar theory. Because science is a collective knowledge, I would also like to express my gratitude to everyone who contributed to the production of all kinds of knowledge that made this research possible.

In a special way, I am thankful to my father, Hasan Cihan Çolak, who is always there to support me and inspire me. I would also like to express my gratitude to Zelal Deniz Demir whose precious friendship helped me to overcome all stressful times, to Elçin Gündogdu Aktürk whose guidance helped me to know myself with her warm friendship and to lovely baby Asya Aktürk, and to my friends who supported me in this process. I am also thankful to METU library workers and to all METU workers who are invisible heroes for creating the peaceful environment for this research. Lastly, I would also thank all the kindhearted and hopeful people of this land and of the world who make life meaningful.

My gratitude also goes to TUBITAK for the scholarship with TUBITAK BIDEB 2210 National Scholarship Programme for MSc Students.

TABLE OF CONTENTS

LIST OF TABLES

TABLES

LIST OF FIGURES

FIGURES

CHAPTER 1

ACCRETING MILLISECOND PULSARS

1.1 Introduction

Millisecond pulsars are objects with spin periods 1.4 ms < P_s < 30 ms, spin-down rates 10^{-19} s s^{-1} and magnetic fields around 10^8 G.

In Figure 1.1, P - $\dot{P}$ diagram of radio pulsars is shown. In the upper right points refer to isolated radio pulsars and open circled points refer to binary radio pulsars Lorimer [2008].

Surface B field strength is direct proportional with spin period and period derivative of the star:

$$B \approx (P\dot{P})^{1/2} \tag{1.1}$$

Characteristic age of the neutron star is calculated by:

$$T_c = P/2\dot{P} \tag{1.2}$$

1.2 Historical Background

After the discovery of Her X-1 in 1974, Bisnovatyi-Kogan & Komberg asserted that accreting neutron stars in binary systems have weak magnetic fields and at the end of the accretion phase hardly observable low luminosity radio pulsars are formed. Besides they claimed that accretion causes decrease in spin period and suppression in magnetic field Alpar [2008].

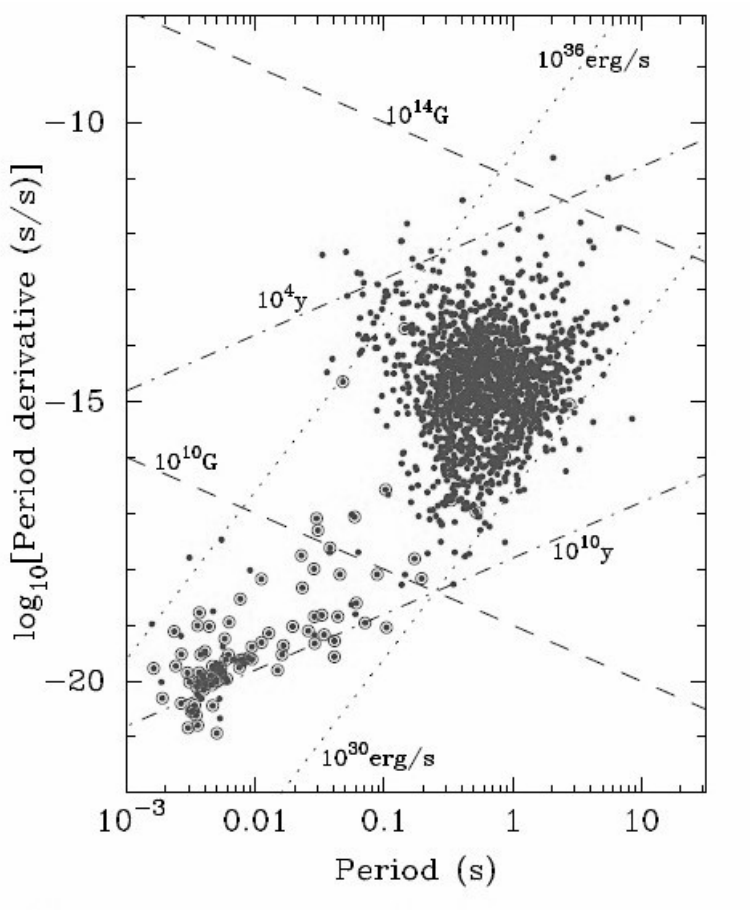

Figure 1.1: Period – Period derivative diagram of radio pulsars Lorimer [2008] Upper right points symbolise isolated radio pulsars and open circled points symbolise binary radio pulsars. Dashed lines indicate magnetic field, dashed-dotted lines indicate characteristic ages and, dotted lines indicate spin-down energy loss rate.

In 1975, first radio pulsar in a binary system PSR B 1913+16 was discovered by Hulse and Taylor. PSR B1916+13 pulsar was also first pulsar positioned out of the pulsar island which is showed in Figure 1.2 Source's short spin period (59ms) indicated that it might be a young pulsar; on the other hand, its weak magnetic field (10^{11} G) implied that it might be an old pulsar Alpar [2008].

In 1982, the first millisecond radio pulsar PSR B 1937+21 was discovered by Backer, Kulkani, Heiles, Davies and Gross. Shortly after this discovery, it was asserted that millisecond pulsars are evolved in LMXBs as a result of accretion at the same time by two independent group Alpar, Cheng, Ruderman, Shaham and Radhakrishnan, Srinivasan Alpar [2008]. These two groups predicted:

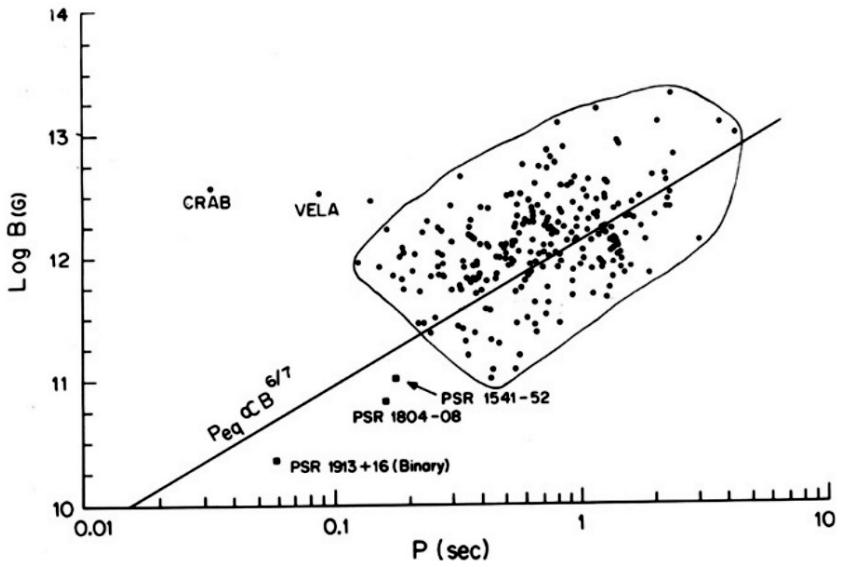

Figure 1.2: Pulsar island of normal pulsars and sources out of this region Srinivasan [2010]. Plot is logarithm of B field in Gauss vs. spin period in second. Upper right region refers to normal pulsars which are evolved from new born stars as Crab and Vela located in upper left part of the plot. The linerepresents equilibrium spin period which is related with $B^{6/7}$. In the lower part of the plot, PSR 1541-52, PSR1804-08 and PSR1913+16 pulsars are located out of the normal pulsar region and PSR1913+16 is the first object that is out of the region and in a binary.

- Magnetic fields should be around 10^8 – 10^9 G,
- Spin-down rate of millisecond radio pulsars should be low as 10^{-19} s s^{-1}.

1.3 Evolution of Millisecond Pulsars

Firstly, the massive star in a binary system turns into neutron star via supernova explosion. Binary is usually disrupted during this explosion and there remain a high velocity isolated neutron star and an OB runaway star. If the binary survived after the explosion, it can be observed as a normal pulsar after 10^7 - 10^8 yr with a spin period higher than a couple of seconds and spin-down Lorimer [2008].

After a while, spin period drops below the critical value and neutron star does not pulsate any more. In the mean time, magnetic field strength of the neutron star will decrease gradually because. If the companion star is massive enough to become a red giant and fill the Roche Lobe, the neutron star accretes matter via RLOF. The neutron

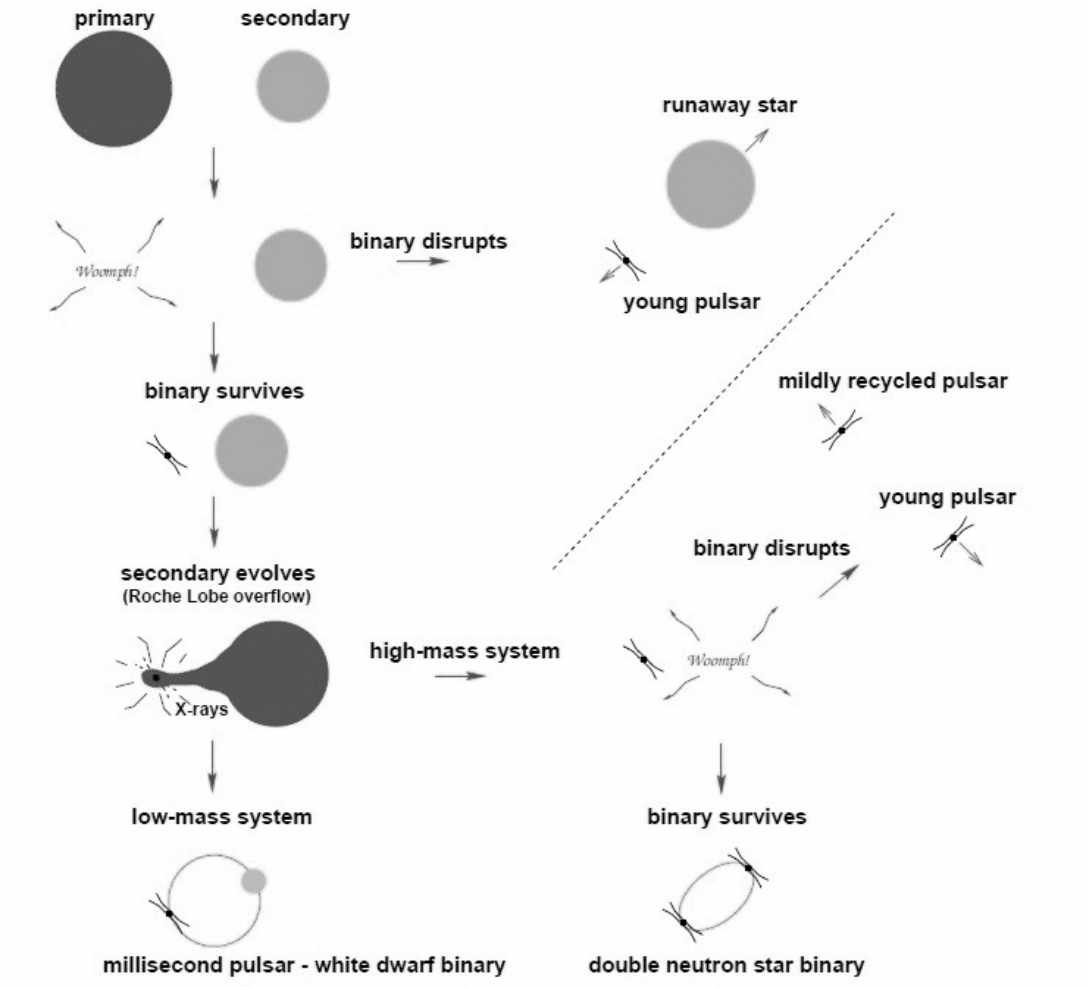

Figure 1.3: Illustration of evolution of binaries Lorimer [2008]. In the diagram, at the beginning binary with a massive star evolves and massive star becomes a neutron star via supernova explosion and most of the binaries disrupted and there remains a young pulsar and a runaway star. If the binary survives and companion is massive enough to accrete matter via RLOF, neutron star spins up and becomes a "recycled pulsar". If the binary system is HMXB, companion star evolved and turn into a neutron star via supernova explosion. After the explosion most binaries disrupted and there remains a young pulsar and a mildly recycled pulsar. If the binary survives, it becomes a double neutron star binary. If the system is LMXB, the neutron star might become a millisecond pulsar via spinning up.

star gains angular momentum in the accretion phase and it starts to spin up. These stars are known as “recycled pulsars” whose evolution diagram can be seen above in Figure 1.3. In the accretion phase, matter falls into the neutron star will be heated by friction and emits x-rays. Thus the system can be observed as a X-ray binary systemSrinivasan [2010].

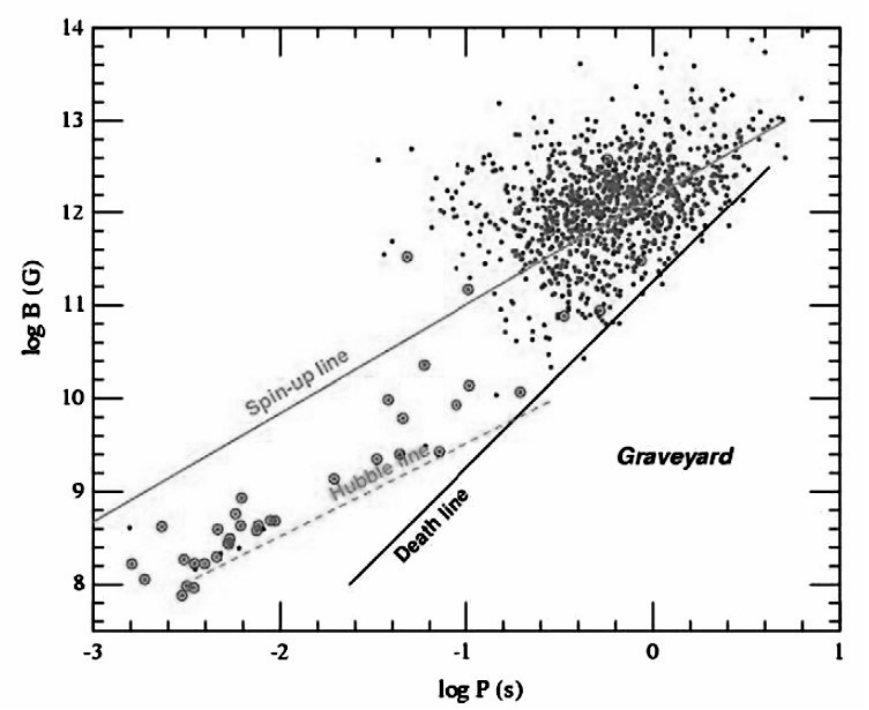

Figure 1.4: Distribution of pulsars in (B-P) plane Patruno [2012].The plot is logarithm of magnetic field in Gauss vs. logarithm os spin period in seconds. In the upper right part of plot, points symbolise normal pulsars and in the middle part of plot, dotted circles symbolise pulsars in HMXB systems and in the lower left part of plot, dotted circles symbolise pulsars in LMXB systems. Lower right part is graveyard location of the pulsars where normal pulsars drop below death line and do not pulsate any more. If they are in a binary system and spin up via accretion, they might pass the death line and become recycled pulsar. Spin up line represents the minimum spin period corresponding to magnetic field and hubble line represents the possible location of the pulsars after one Hubble time which is about 10^{10} years.

According to the mass of the companion star there are three possible evolution paths for the binary which consists of a recycled neutron star and a companion.

1) If the system is HMXB (companion star in the system $M_c > 10\ M\odot$, might be massive white dwarf (WD),neutron star (NS) or main sequence star (MS) and eccentricity $0.15 < e < 0.9$) the recycled neutron star will have a lower B field and smaller spin periods compared with normal pulsars. On the other hand, these pulsars can not reach around 10^8 G B field strength and millisecond spin periods because high accretion rates of HMXBs do not allow the pulsar to attain lower values, therefore they locate between normal pulsars and LMXB millisecond pulsars in B-P plane which

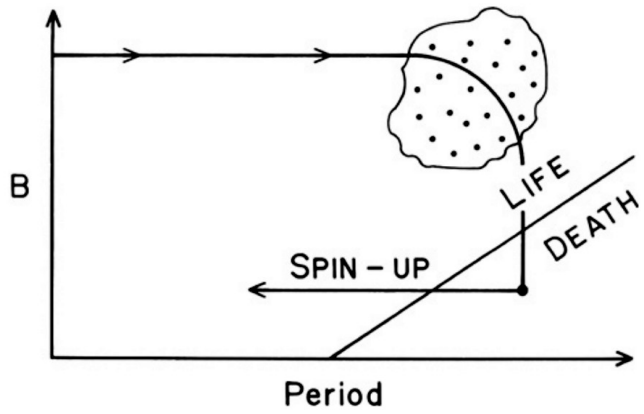

Figure 1.5: Evolution diagram of recycled pulsars Srinivasan [2010]. In the logarithm of magnetic field in Gauss vs. spin period in seconds diagram, spin period of newborn pulsars decrease after supernova explosion and they locate in normal pulsar region. With magnetic field suppression, they go beyond from life region to death region and stop pulsating. If the pulsars are in a binary and spin up, they might exceed the life limit and pulsate again.

is shown in Figure 1.4. These recycled pulsars are mostly observed as radio pulsars Lorimer [2008].

After companion star evolved enough to turn into neutron star via supernova explosion, binary will be distrusted usually by the explosion and there remain a mildly recycled pulsar and a young neutron star. Isolated recycled pulsars in recycling phase can be explained by this way. With low probability, binary survived after the explosion and the system become double neutron star binary Lorimer [2008].

In Figure 1.5 blue points illustrate normal pulsars. Recycled pulsars locate below the normal pulsars and illustrated with red points. Recycled pulsars form two distinct groups: 1) Recycled pulsars with massive companions which have higher B fields and longer spin periods. 2) Recycled pulsars with low mass companions which have lower B fields and shorter spin periods Patruno [2012].

2) If the system is LMXB(companion star in the system $M_c < 0.7\ M\odot$, dominantly white dwarf (WD), and eccentricity $10^{-15} < e < 0.01$), companion star become a white dwarf (WD) with a high probability. Accretion phase continues until the companion become white dwarf. Because accretion rates are low enough to provide a long timescale for spin up of the neutron star in LMXBs, its spin period might reach to mil-

liseconds and might be observed in radio wavelength as "radio millisecond pulsars" or x-ray wavelength as accreting millisecond pulsars Lorimer [2008]. The accretion depend on the radius of the inner edge of accretion disc which is called Alfven radius and the corotation radius of the neutron star Srinivasan [2010].

$$R_A = (B^2 R^{12}/8GM\dot{M}_a^2)^{1/7} \text{ (Alfven Radius)} \tag{1.3}$$

$$R_C = (GM/\Omega^2)^{1/3} \text{ (Corotation Radius)} \tag{1.4}$$

- If Alfven radius is higher than corotation radius ($R_A > R_C$), the matter is expelled and accretion does not take place.
- If radius is lower than corotation radius ($R_A < R_C$), the matter will accrete until these two radii will be equal ($R_A = R_C$). Within this period, spin period of the neutron star will decrease by spin-up until equilibrium spin period is gained which is Keplerian period at inner edge of accretion disc.

$$P_{eq} \propto B^{-6/7}\dot{M}^{-3/7} \text{ (Keplerian Period)} \tag{1.5}$$

Upper limit of Eddington luminosity limit for accretion rate limits the minimum value of equilibrium period, P_{eq}

$$P_{eq} = 1.9ms(B/10^9 G)^{6/7} \text{ (Eddington limited minimum } P_{eq}) \tag{1.6}$$

This relation allows a successful determination of spin period of PSR B 1913+16 which is observationally found as 59ms. The evolution diagram of the object can be seen in Figure 1.6 above.

1.4 Properties of Accreting Millisecond Pulsars

Accreting millisecond x-ray pulsars are objects with spin periods $P_s > 100$ Hz. They are bounded in LMXB systems and their mass of companion stars are lower than 1 $M\odot$. Their orbital periods are shorter than 1 day and magnetic fields are about B 10^{8-9} G. They have accretion discs and mass transfer from the companion star occurs via Roche Lobe overflow (RLOF) Patruno [2012]

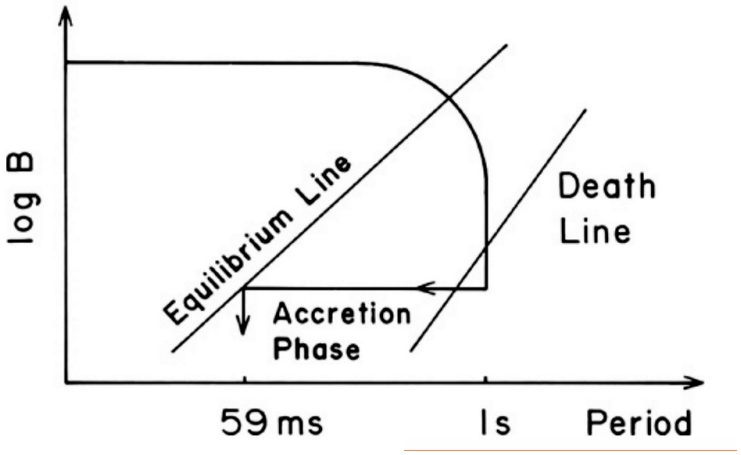

Figure 1.6: Evolution diagram of PSR B 1913+16 Srinivasan [2010].In the logarithm of magnetic field in Gauss vs. spin period in seconds diagram, evolution path of PSR B 1913+16 is shown. It is thought that the pulsar followed the recycled pulsar's path and in accretion phase it spun up until it reached to equilibrium line. Theoretical prediction for spin period of PSR B 1913+16 was 59 ms which matches with observational results.

Accreting millisecond x-ray pulsars are transient systems which have quiescence and outburst phases. In quiescence phase luminosity is about 10^{31-33} erg s^{-1} and in outburst phase x-ray luminosity can reach to values about 10^{36-37} erg s^{-1} Falanga [2012]. This faint luminosity during outbursts indicates to low averaged mass accretion rates Patruno [2012]. Coherent x-ray pulsations between 182-599 Hz are observed in outburst phases Falanga [2012].

14 accreting millisecond x-ray pulsars are observed so far. 3 of them are intermittent accreting millisecond pulsars. In these sources typical AMSP pulsations observed in the beginning of the outbursts but then they become intermittent which means the pulsations are appearing and disappearing on different timescales. Intermittent accreting millisecond pulsars are thought as the link between pulsing and non-pulsing systems. Amplitudes of the pulsations are small and they show highly sinusoidal waveform Patruno [2012].

Accreting millisecond x-ray pulsars shows x-ray oscillations in millisecond periods which are originated from three reason. First of them is accretion powered oscillations which are caused by rotation of the pulsar. Periods of oscillations and the spin period of the source are equal. Second of them is nuclear powered burst oscillations which

are caused by thermonuclear bursts. Periods of the oscillations and spin period of the source are very close. Third of them is kHz Quasi Periodic Oscillations (QPOs) which are caused when accreting material in low magnetic field sources could not reach to magnetic poles and get closer to surface of the source.

1.4.1 Thermonuclear Bursts

1.4.1.1 General Properties

Thermonuclear bursts, which are also called Type I X-ray bursts, are thermonuclear explosions triggered by unstable burning of H or He on the layers of neutron stars. The imbalance between nuclear heating and radiative cooling causes these bursts. They burn their fuel about 10 - 100 seconds, their mass donors are typically old, Population II objects or degenerate He or C/O white dwarfs Patruno [2012].

1.4.1.2 Physics of Thermonuclear Bursts

In the accreting neutron stars, H and He accretion onto their surface causes hydrostatic compression and within a few hours temperature conditions and ignition densities can be achieved. Unstable burning of H or He can trigger thermonuclear bursts Patruno [2012].

According to Strohmayer and Bildsten Strohmayer [2006], expected unstable burning in thermonuclear bursts can be divided into 3 regimes. Compression rate is defined as accretion rate per unit area: $\dot{m} = \dot{M}$ /A_{acc} (area covered by fresh material, A_{acc}, is about 1.2×10^{13} cm^2).

1) Mixed H and He burning triggered by thermally unstable H ignition for $\dot{m}$ < 900 g cm^2 s^{-1} ($\dot{M}$ < 2 $\times$ 10^{-10} M$\odot$ yr^{-1})

Accretion onto the atmosphere increases temperature to 107 K and this temperature provides H to burn in the CNO cycle. After the temperature exceeded 8×10^7 K, H started to burn in "hot" CNO cycle Fowler [1965].

$$^{12}C(p,\gamma)^{13}N(p,\gamma)^{14}O(\beta+)^{14}N(p,\gamma)^{15}O(\beta+)^{15}N(p,\alpha)^{12}C \tag{1.7}$$

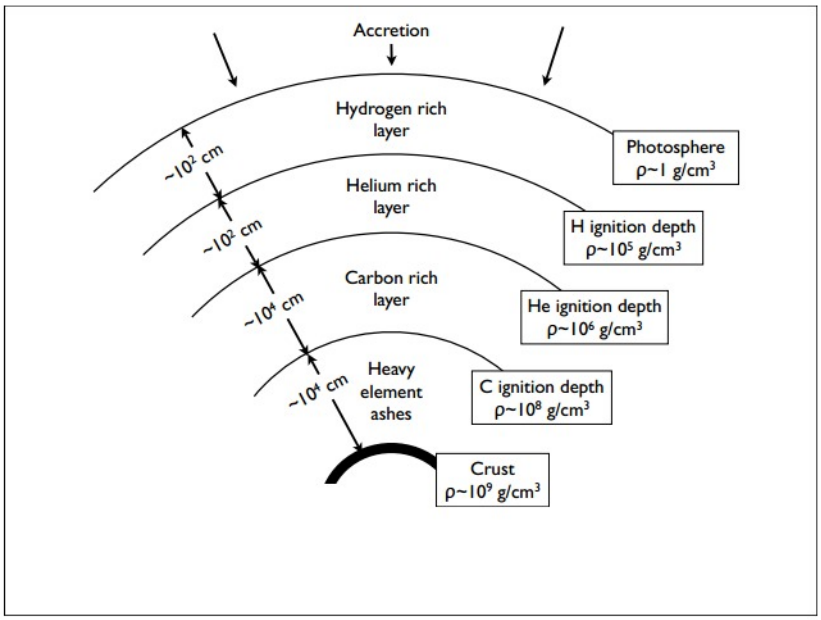

Figure 1.7: Outer layers of accreting neutron stars and ignition densities for thermonuclear burning Patruno [2012]. Approximate thickness of the layers are given in cm and approximate ignition depths are given in g/cm^3.

When the accretion rate is higher than 900 g cm^2 s^{-1} , H burning in hot CNO cycle is stable. If the accretion rate drops below 900 g cm^2 s^{-1}, H burning became thermally unstable which can cause thermonuclear bursts.

2) Pure He shell ignition for 900 g cm^2 s^{-1} < $\dot{m}$ < 2 $\times$ 10^3 g cm^2 s^{-1} following completion of H burning

In this accretion rate interval, H continues to burn stably until it finishes, meanwhile pure He shell maintains to accrue. When the temperature decreased below 5 $\times$ 10^8 K and thin shell density condition for He layer provided, He burning became thermally unstable and pure He flashes occur in the lack of H.

He flashes caused by unstable He burning increase the temperature and "breakout" reactions can start:

$$^{15}O(\alpha,\gamma)^{19}Neand^{18}Ne(\alpha,p)^{21}Na \tag{1.8}$$

By these reactions, H no longer burns in CNO cycle and burning of H begins in rp process which consists of proton captures and beta decays. A large range of heavy nuclei, which is showed in Figure 1.8, is produced by the rp process Schatz [2001]

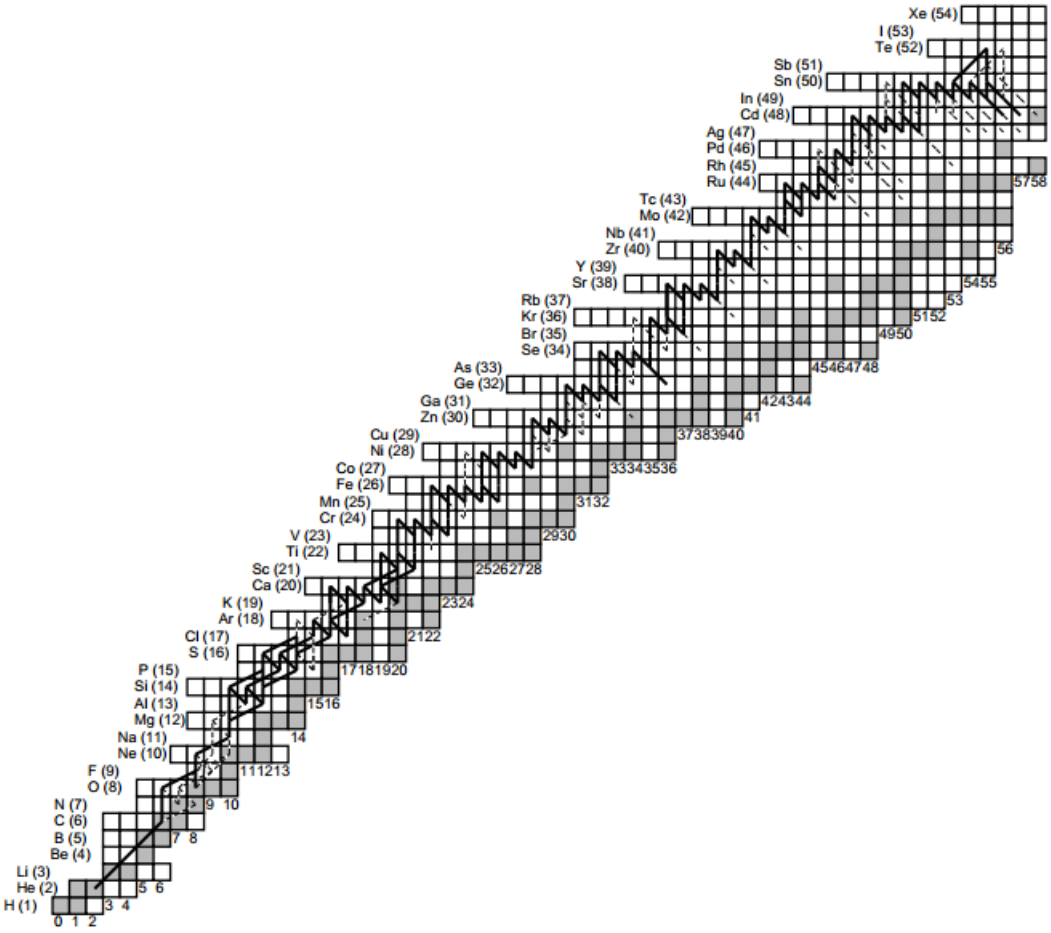

Figure 1.8: Dominant pathways of nuclear reaction flows during rapid-proton (rp) process Strohmayer [2006].Elements and their atomic numbers are given beside the pathways. With proton captures and beta decays via rp process, H can burn until large range of heavy nuclei produced.

and they can be observed in burst spectra.

3) Mixed H and He burning triggered by thermally unstable He ignition for $\dot{m}$ > 2×10^3 g cm^2 s^{-1} ($\dot{M}$ > 4.4×10^{-10} M$\odot$ yr^{-1})

The accretion rate exceeded 2×10^3 g cm^2 s^{-1} and density condition for He burning is satisfied before slow H burning finished in the above layer, H and He burning start to occur at the same time. When the temperature decreased below 5×10^8 K which causes unstable He burning, thermonuclear bursts can be observed.

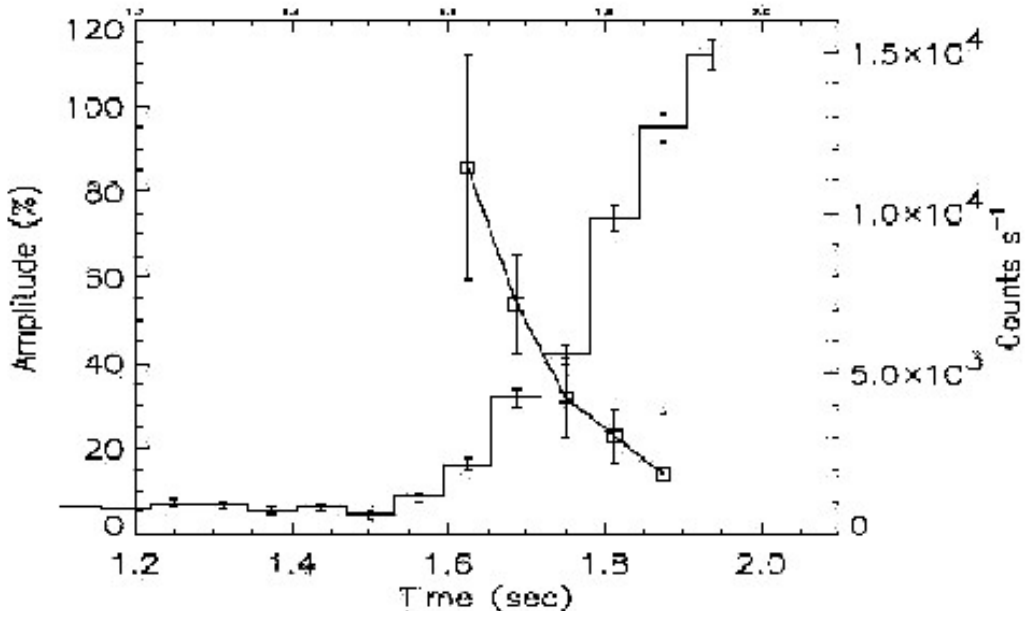

Figure 1.9: Oscillations amplitudes of 4U 636-53 during burst rising phase. In the x-axis of the plot time is given in seconds. In the y-axis percent range for oscillation amplitude changes and in the left and count/s range for lightcurve of the burst rising in the right. Squares represent average values of counts per second.

1.4.1.3 Burst Oscillations

During thermonuclear bursts, some sources show frequency shifts between 300 – 500 Hz which are called burst oscillations. Burst oscillation properties changes according to type of neutron star and matter accretion rates but bursts have some common properties. Firstly, their burst rise times are generally 1-2 seconds and decay times are generally between 10 seconds to several minutes. Secondly, burst profiles are shorter in higher energies caused by cooling of neutron star. Thirdly, burst profiles generally show smooth, exponential or exponential like decays. Fourthly, oscillation amplitudes are inversely proportional to flux, when flux increases, oscillation amplitudes decrease as shown in Figure 1.9. Fifthly, there is a close relation between burst frequency and spin frequency Strohmayer [2006].

Fourth and fifth properties indicate a localized hotspot. Largest modulations are seen when the hotspot is smallest at the burst onset and with expansion of the hotspot amplitudes decreases. This condition also can be observed in bolometric flux vs

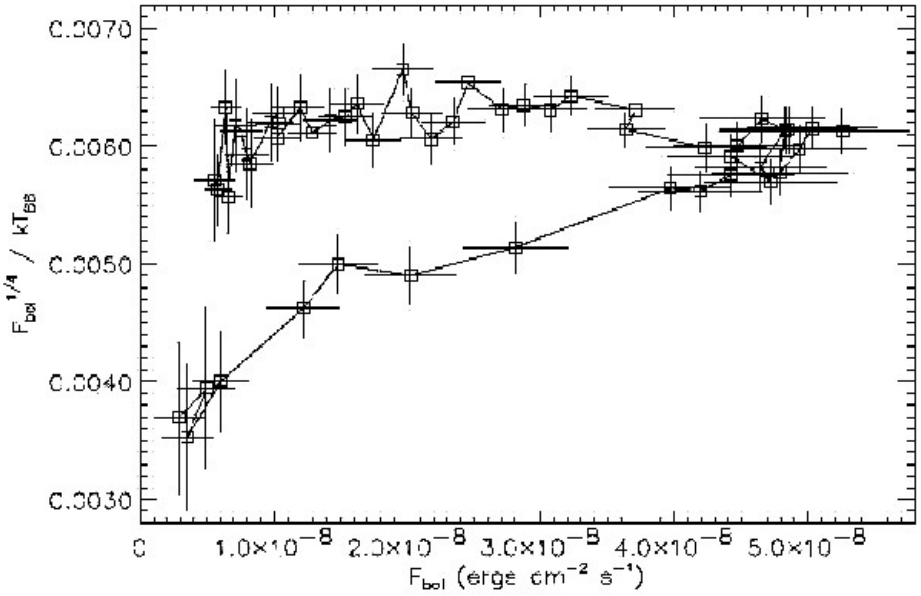

Figure 1.10: F_{bol} vs F_{bol}/kTbb plot of 4U 1728-34. Bolometric flux is given in erg cm^{-2} s^{-1}. Burst starts from lower left and continues to upper right and then to the left Strohmayer [2006].

bolometric flux/blackbody temperature diagrams which can be seen in Figure 1.10 Strohmayer [2006].

In addition, fuel accretion takes hours but it burns in a few minutes which supports the idea that burst cannot happen simultaneously on the entire surface of neutron star. There are two model to explain the thermonuclear bursts. One of them is hot spot model and the other one is surface mode model Watts [2012].

1) **Hotspot Model:** Thermonuclear burning does not take place homogenously on the neutron stars surface but it occurs in a small region and this causes burst oscillations as neutron star rotates. There are two hotspot model: "spreading hotspot" which is formed temporarily in rise as burst ignites and flame spread from the ignition site to engulf star and "persistent hotspot" which is caused by restriction of burning to small part of stellar surface Watts [2012].

2) **Surface Mode Model:** Ignition of burst and subsequent spread of flame around the star may excite large-scale waves(global waves) in neutron stars surface. Height difference associated with such oscillations would translate into hotter and cooler patches (wave pattern), thus giving rise to difference in X-ray

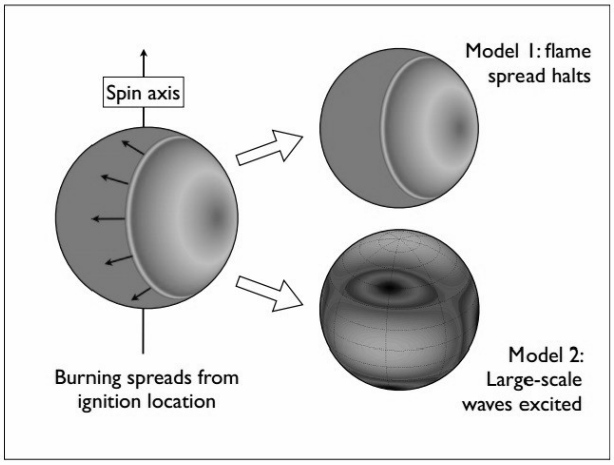

Figure 1.11: Illustration of hotspot and surface mode models Watts [2012]. After burning spreads from ignition location, flame spread might halt which is hotspot model and large scale waves might be excited which is surface model.

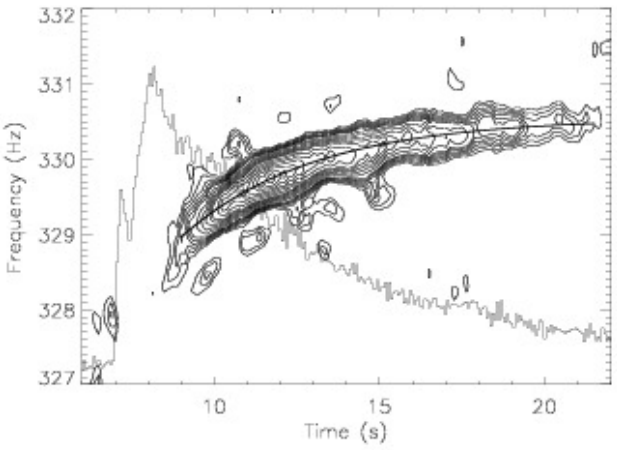

Figure 1.12: Dynamical power spectrum of 4U 1702-429. The plot is given in frequency in Hz vs. time in seconds. Contours show frequency shifts with respect to burst light curve Strohmayer [2006].

brightness which can be shown in Figure 1.11 Watts [2012].

Moreover, some sources show spin evolution during their burst oscillations which can be seen in Figure 1.12. These shifts in spin frequencies are caused by photospheric radius expansion (PRE) period. During these periods the photosphere of neutron star is heated and it expands. With rotation of neutron star, spin frequency shifts can be observedStrohmayer [2006].

CHAPTER 2

OBSERVATIONS AND DATA ANALYSIS

2.1 RXTE

Rossi X-ray Timing Explorer (RXTE) had started its mission on December 30, 1995 and ended on January 5, 2012. NASA's Goddard Space Flight Center (GSFC) organised the mission especially for high time resolution observations of X-ray sources. Its spectral range is between 2 to 250 keV. It consists of two pointed instruments which are the Proportional Counter Array (PCA) and High Energy X-ray Timing Experiment (HEXTE). Moreover, there exists an All-Sky Monitor (ASM) on it.

In Figure 2.1, PCA, HEXTE and ASM instruments can be seen.

2.2 Software Used in Pulse Phase Resolved Spectroscopy

In the pulse phase resolved spectroscopy analysis of each sources, Good Xenon 1 and 2 modes of PCA instrument are selected. "FTOOLS" softwares of HEASARC/-NASA are used in the data reduction. Good time intervals are created via "xtefilt" and "maketime". For phase resolved spectroscopy, "fasebin" , "fbssum" are used. For total spectrum of Good Xenon data modes "seextrct" is used. For background subtraction, Standard 2f data mode is used and subtraction is done via "pcabackest" and "saextrct". For lightcurves are produced from Standard 2f or Good Xenon data mode. For spectrum modelling "xspec" is used.

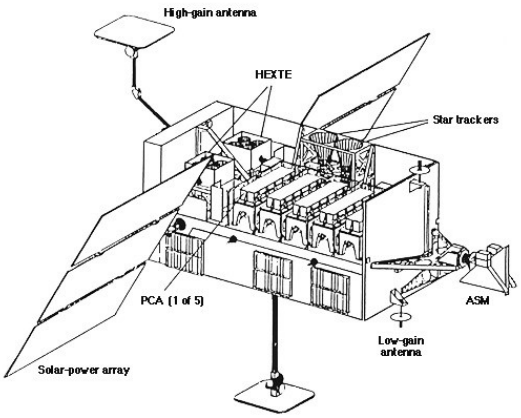

Figure 2.1: RXTE spacecraft diagram.

2.3 Phase Resolved Spectroscopy of XTE J0929-314

XTE J0929-314 is discovered on April 13, 2002 Remillard [2002]. Its spin frequency is 185 Hz and its orbital period is 43.6 minutes. Its minimum companion mass is 0.01 M_s and companion type is cold He white dwarf Patruno [2012].

XTE J0929-314 has showed only one outburst in 2002 and it lasted about 52 days but only 34 days observed by RXTE/PCA Patruno [2012]. Light curve of the source can be seen in Figure 2.2. Also total pulse obtained from all data is shown in Figure 2.3. Total spectrum obtained from all data is given below in Figure 2.4 . In the modelled spectrum, nH value is fixed at 0.76×10^{21} cm^{-2} and blackbody temperature is about 0.69 keV and photon index is about 1.8.

Position of the source is used as R.A : 9^h 29^m $20^s.19$ and DEC. : -31^o 23' 3".2 Giles [2005] for the analysis and timing parameters of the system is used as orbital period P_{orb} : 2614.746(s) , spin period P_s : 185.105254297(Hz) , projected semimajor axis $a_x$sini 6.29(light-ms) and epoch of spin frequency t_0 : 52396.0(MJD) Galloway [2002].

Results of pulse phase resolved x-ray spectroscopy of XTE J0929-314 is given in Figure 2.5

In the results of phase resolved spectroscopy analysis of XTE J0929-314 during 2002 outburst, significant negative correlation is found between photon index and black-

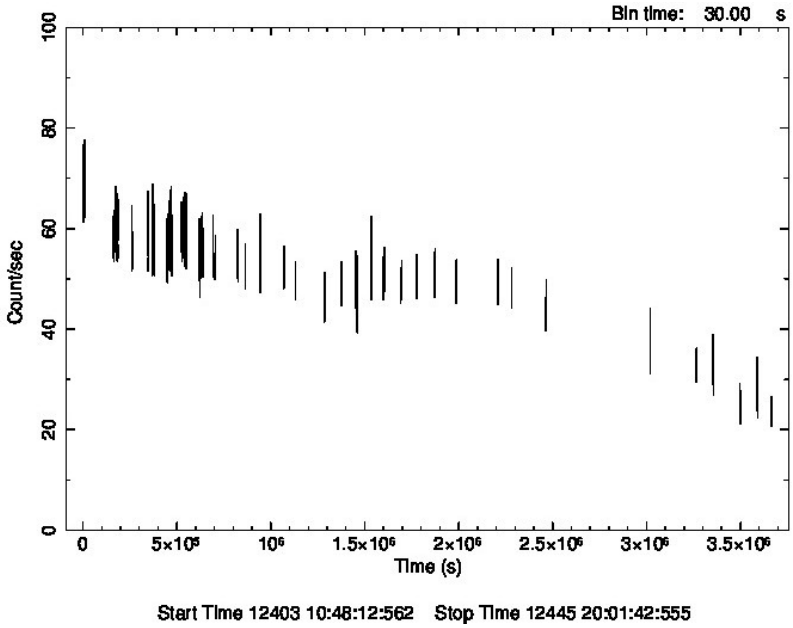

Figure 2.2: 2002 outburst Lightcurve of XTE J0929-314. Plot is given in count per second vs. time in seconds. The lightcurve extracted from Standard 2f data mode

body temperature at the rate of -0.938 Pearson correlation constant. Pearson coefficient values are calculated from average values of each parameter. Results of Pearson

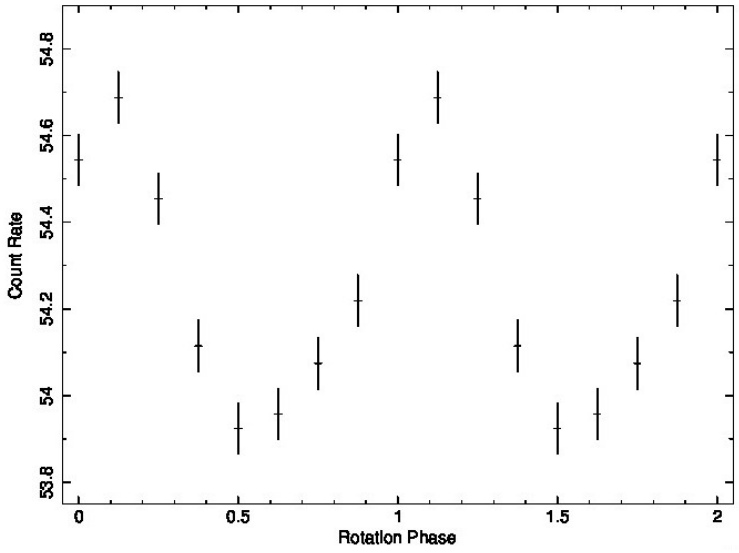

Figure 2.3: Total pulse of XTE J0929-314 during 2002 outburst. Pulse is extracted from all data used for the phase-resolved analysis. Plot is given in count rate vs. rotation phase which represents twice rotation. In the x-axis, rotation phase is equals to 1 when the source rotated 360^o and pulse is plotted with 2 rotation phase.

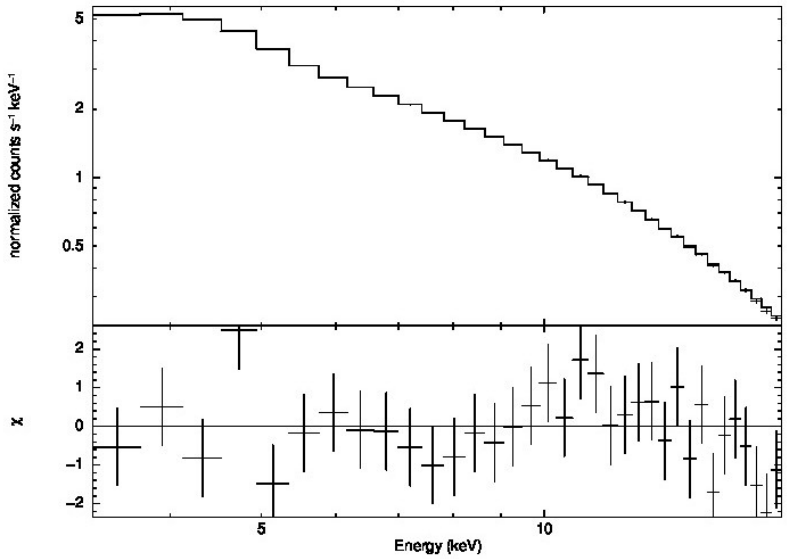

Figure 2.4: Total spectrum of XTE J0929-314 during 2002 outburst. Spectrum is extracted from all data in Good Xenon mode which are also used in phase-resolved spectroscopy. Spectrum fitted well with blackbody + power law models and nH is fixed at 0.76×10^{21} cm^{-2}, blackbody temperature is found about 0.69keV and photon index is found about 1.8 .

correlation coefficient calculations are given below in Table 2.1. Photon index vs. flux plot is given below in Figure 2.6.

All phase spectra can be found in Appendix A section and all observations id's used in the analysis can be found in Appendix B.

Table 2.1: Correlation Table of XTE J0929-314 during 2002 outburst. Y-axis of the first panel is flux in 10^{-10} erg per cm^2 s^{-1}, y-axis of the second panel is blackbody temperature in keV, y-axis of the third panel is photon index and y-axis of the fourth panel is reduced chi^2. X-axis of all panels are rotation phase and the source is divided into 8 rotational phases for the analysis.

	Flux-Blackbody	Flux-Photon Index	Blackbody-Photon Index
Pearson Correlation	-.166	.335	-.938**
Sig.(2-tailed)	.695	.417	.001
N	8	8	8

** Correlation is significant at the 0.01 level (2-tailed)

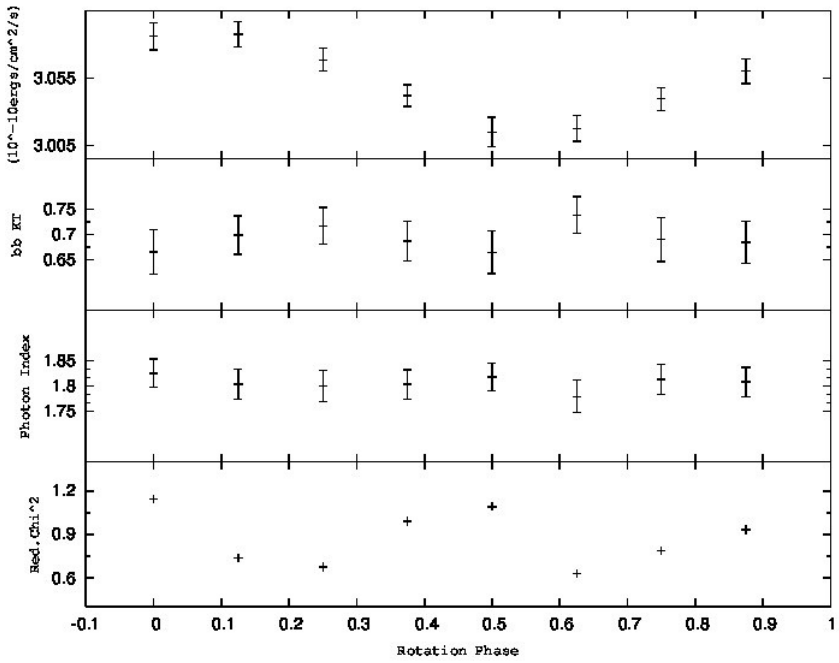

Figure 2.5: Results of Pulse Phase-Spectroscopy of XTE J0929-314 during 2002 outburst. Y-axis of the first panel is flux in 10^{-10} erg per cm^2 s^{-1}, y-axis of the second panel is blackbody temperature in keV, y-axis of the third panel is photon index and y-axis of the fourth panel is reduced chi^2. X-axis of all panels are rotation phase and the source is divided into 8 rotational phases for the analysis.

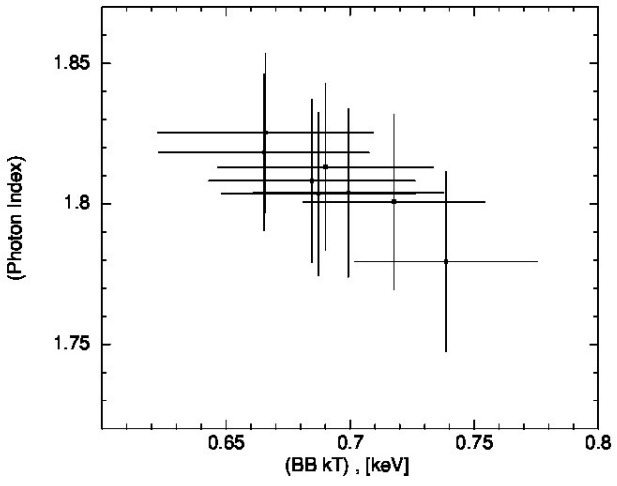

Figure 2.6: Blackbody Temperature vs. Photon Index plot of XTE J0929-314 during 2002 outburst. With Pearson correlation calculations blackbody temperature, flux and photon index parameters are compared with each other and negative correlation between blackbody temperature and photon index is found for the source.

2.4 Phase Resolved Spectroscopy of IGR J00291+5954

IGR J00291+5954 is discovered on December 2, 2004 Eckert [2004]. Its spin frequency is 599 Hz which can be seen in its power spectrum in Figure 2.7. Its orbital period is 2.46 hour. Its companion mass is higher than 0.04 M_s and companion type

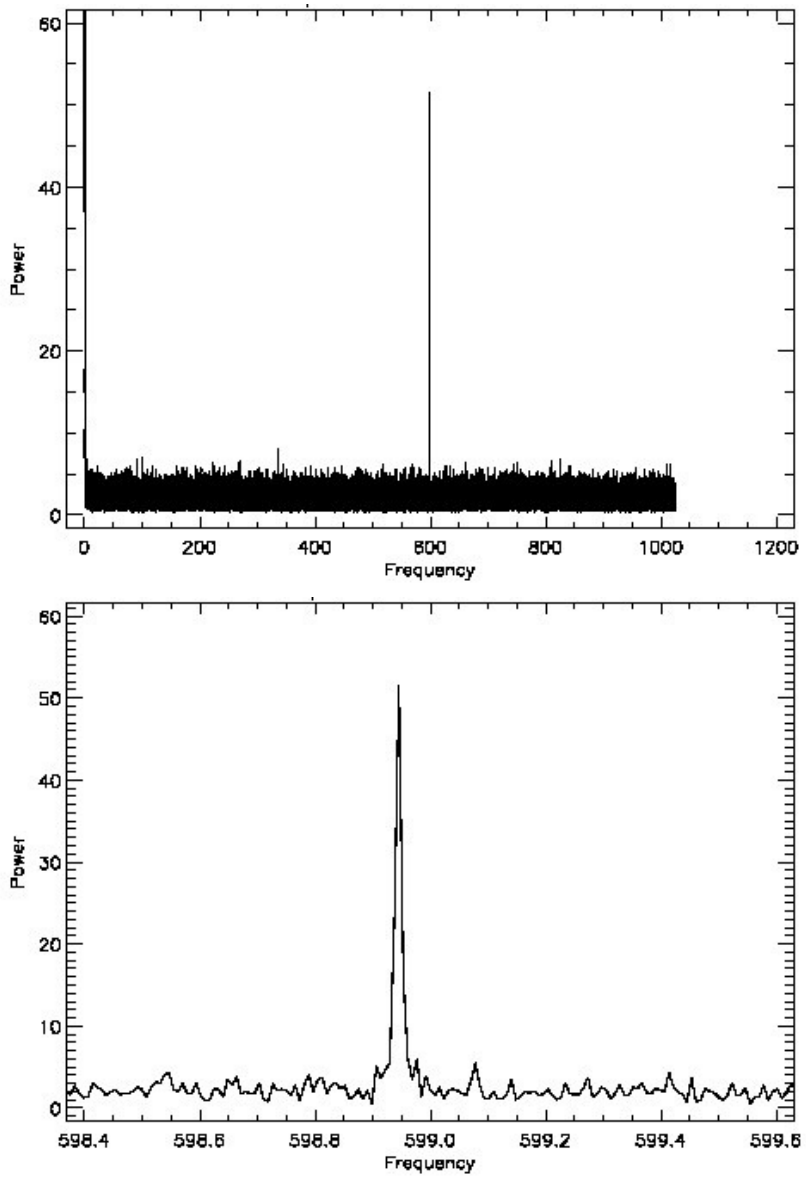

Figure 2.7: Power spectrum (upper panel) and rescaled power spectrum (bottom panel) of IGR J00291+5954. As a result of IDL analysis of the source, plots are given in power vs. frequency. The sharp pulse can be seen in rescaled power spectrum as 598.9 Hz which is consistent with spin period of the source.

is a brown dwarf Patruno [2012].

IGR J00291+5954 has three outbursts in December 2004, August 2008 and September 2008. December 2004 outburst has 14 days duration and smooth decay observed in its flux. In addition to 2004 outburst, the source is observed in August 2008 again. This outburst started on August 13 and lasted about one week. August 2008 peak flux was about half of 2004 outburst peak flux. Follow up Swift/XRT observations on August 21 showed that flux level is below 10^{-11} erg/s. Also XMM-Newton observations on August 25 confirmed that flux level is below 10^{-14} erg/s which are consistent with 2004 quiescence flux level about 10^{-13} erg/s Patruno [2012]. In September 2008 source is detected again.The outburst started on September 21 and observed about 14 days. August and September flows are very similar and it is unclear that whether two outbursts distinct or part of the same outbursts Patruno [2012].

2008 September outburst is analyzed and light curve of it is in Figure 2.8. Good Xenon data mode of RXTE/PCA is used which is between 54732.338 MJD and 54740.106 MJD. In Figure 2.9, total pulse of all data is shown.

Total spectrum obtained from all data is given below in Figure 2.10 . In the modelled spectrum, nH value is fixed at 5×10^{21} cm^{-2} and blackbody temperature is about 0.9

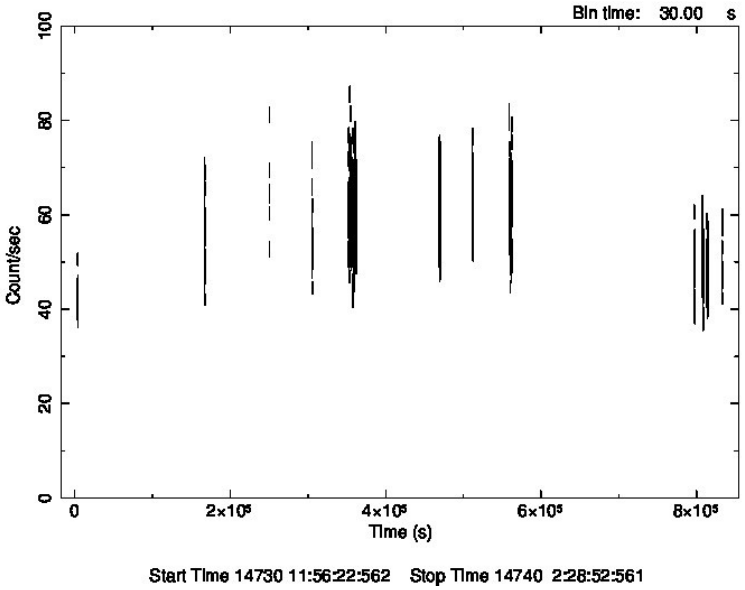

Figure 2.8: 2008 September outburst Lightcurve of IGR J00291+5954. Plot is given in count per second vs. time in seconds. The lightcurve extracted from Standard 2f data mode

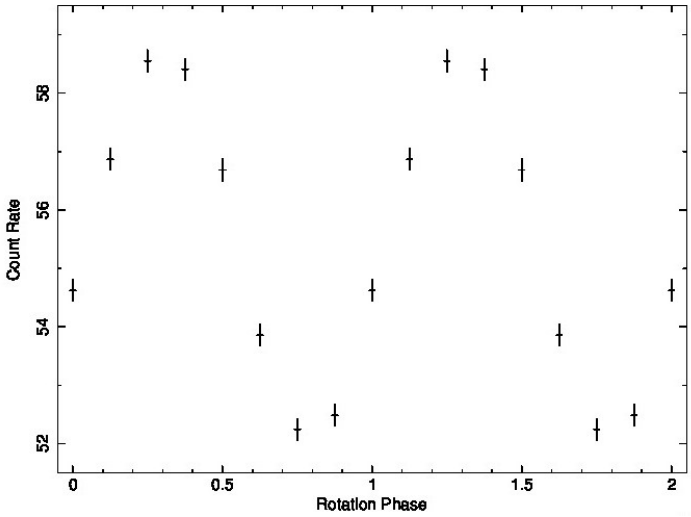

Figure 2.9: Total pulse of IGR J00291+5954 during 2008 September outburst. Pulse is extracted from all data used for the phase-resolved analysis. Plot is given in count rate vs. rotation phase which represents twice rotation. In the x-axis, rotation phase is equals to 1 when the source rotated 360^o and pulse is plotted with 2 rotation phase.

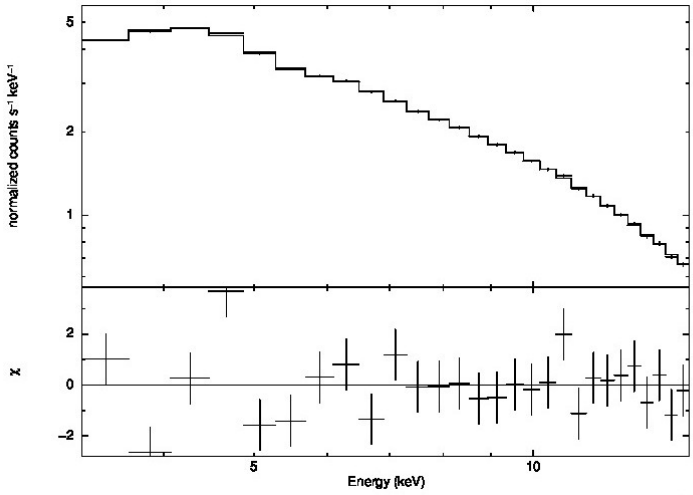

Figure 2.10: Total spectrum of IGR J00291+5954 during 2008 September outburst. Spectrum is extracted from all data in Good Xenon mode which are also used in phase-resolved spectroscopy. Spectrum fitted well with blackbody + power law models and nH is fixed at 5×10^{21} cm^{-2}, blackbody temperature is found about 0.9keV and photon index is found about 1.6 .

keV and photon index is about 1.6.

Position of the source is used as R.A : 00^h 29^m 03^s.05 and DEC. : $+59^o$ 34' 18".93 Torres [2008] for the analysis and timing parameters of the system is used as orbital

period P_{orb} : 8844.078(s) , spin period P_s : 598.89213082(Hz) , projected semimajor axis $a_x$sini 64.982(light-ms) and epoch of spin frequency t_0 : 54730.529222(MJD) Papitto [2011a].

Results of pulse phase resolved x-ray spectroscopy of IGR J00291+5954 is given in Figure 2.11

In the results of phase resolved spectroscopy analysis of IGR J00291+5954 during 2008 September outburst, significant relation between blackbody temperature, photon index and flux is not found. Pearson coefficient values are calculated from average values of each parameter. Results of Pearson correlation coefficient calculations are given in the table below in Table 2.2

All phase spectra can be found in Appendix A section and all observations id's used in the analysis can be found in Appendix B.

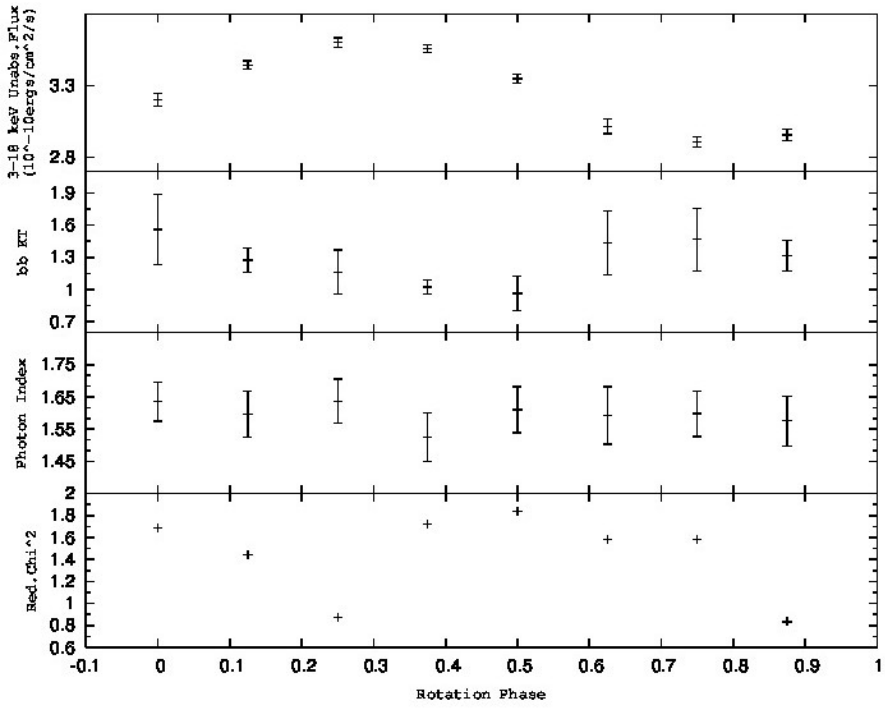

Figure 2.11: Results of Pulse Phase-Spectroscopy of IGR J00291+5954 during 2008 September outburst. Y-axis of the first panel is flux in 10^{-10} erg per cm^2 s^{-1}, y-axis of the second panel is blackbody temperature in keV, y-axis of the third panel is photon index and y-axis of the fourth panel is reduced chi^2. X-axis of all panels are rotation phase and the source is divided into 8 rotational phases for the analysis.

Table 2.2: Correlation Table of IGR J00291+5954 during 2008 September outburst

	Flux-Blackbody	Flux-Photon Index	Blackbody-Photon Index
Pearson Correlation	-.674	.023	-.360
Sig.(2-tailed)	.067	.957	.381
N	8	8	8

** Correlation is significant at the 0.01 level (2-tailed)

2.5 Phase Resolved Spectroscopy of IGR J17498-2921

IGR J17498-2921 is discovered on August 11, 2011 Gibaud [2011]. Its spin frequency is 401 Hz which can be seen in its power spectrum in Figure 2.12. Its orbital period is 3.8 hour. Its companion mass is higher than 0.17 M_s and companion type is a main sequence star Patruno [2012].

IGR J17498-2921 has showed only one outburst in 2011 and it lasted about 40 days Patruno [2012]. Light curve of the source can be seen in Figure 2.13. Also total pulse obtained from all data is shown in Fig 2.14

Total spectrum obtained from all data is given below in Figure 2.15 . In the modelled spectrum, nH value is fixed at 1.2 $\times$ 10^{22} cm^{-2} and blackbody temperature is about 1.5 and photon index is about 1.8. Results of pulse phase resolved x-ray spectroscopy of IGR J17498-2921 is given in Figure 2.16

Position of the source is used as R.A : 17^h 49^m 55^s.35 and DEC. : -29^o 19' 19".6 Papitto [2011b] for the analysis and timing parameters of the system is used as orbital period P_{orb} : 13835.619(s) , spin period P_s : 400.99018734(Hz) , projected semimajor axis $a_x$sini 0.365165(light-ms) and epoch of spin frequency t_0 : 55785.0600534(MJD) Papitto [2011b].

Results of pulse phase resolved x-ray spectroscopy of IGR J17498-2921 is given in Figure 2.16

In the results of phase resolved spectroscopy analysis of IGR J17498-2921 during 20011 outburst, positive correlation is found between photon index and flux at the rate of 0.899 Pearson correlation constant. Pearson coefficient values are calculated

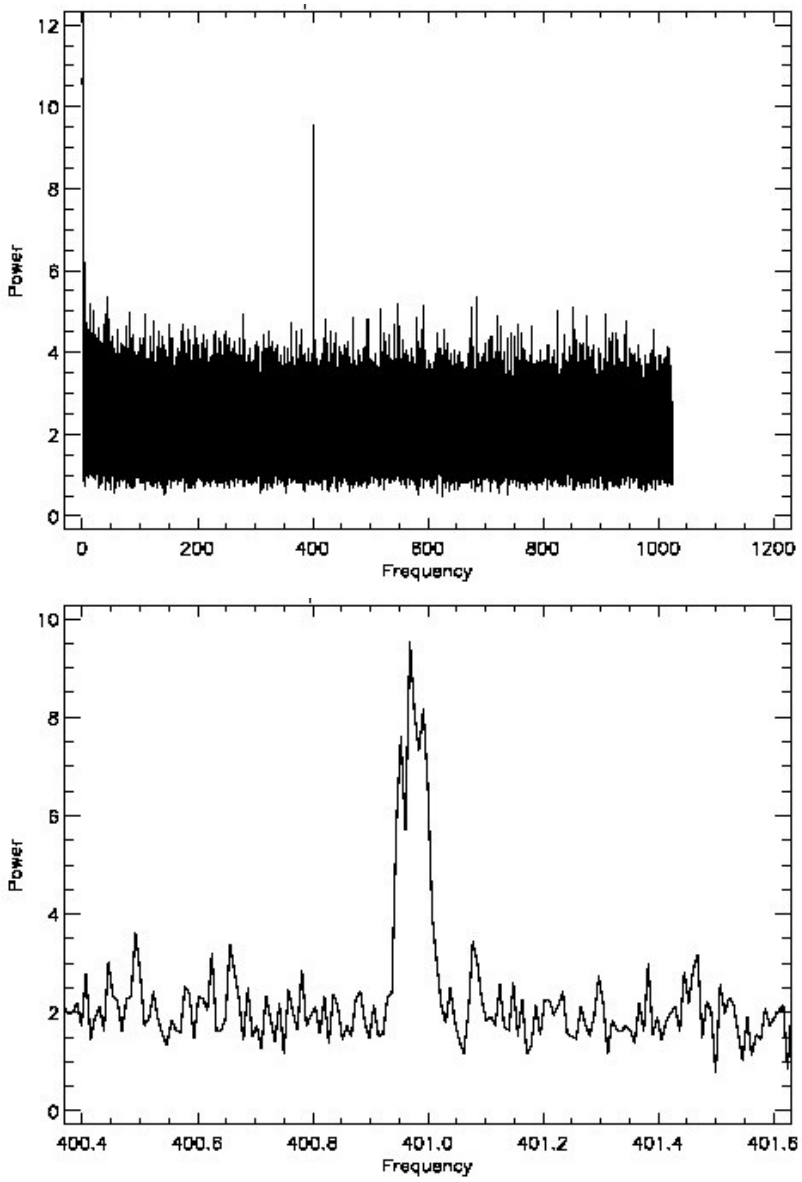

Figure 2.12: Power Spectrum (upper panel) and rescaled power spectrum (bottom panel) of IGR J17498-2921. As a result of IDL analysis of the source, plots are given in power vs. frequency. The sharp pulse can be seen in rescaled power spectrum as 400.95 Hz which is consistent with spin period of the source.

from average values of each parameter. Results of Pearson correlation coefficient calculations are given below in Table 2.3. Photon index vs. flux plot is given below in Figure 2.17.

All phase spectra can be found in Appendix A section and all observations id's used in the analysis can be found in Appendix B.

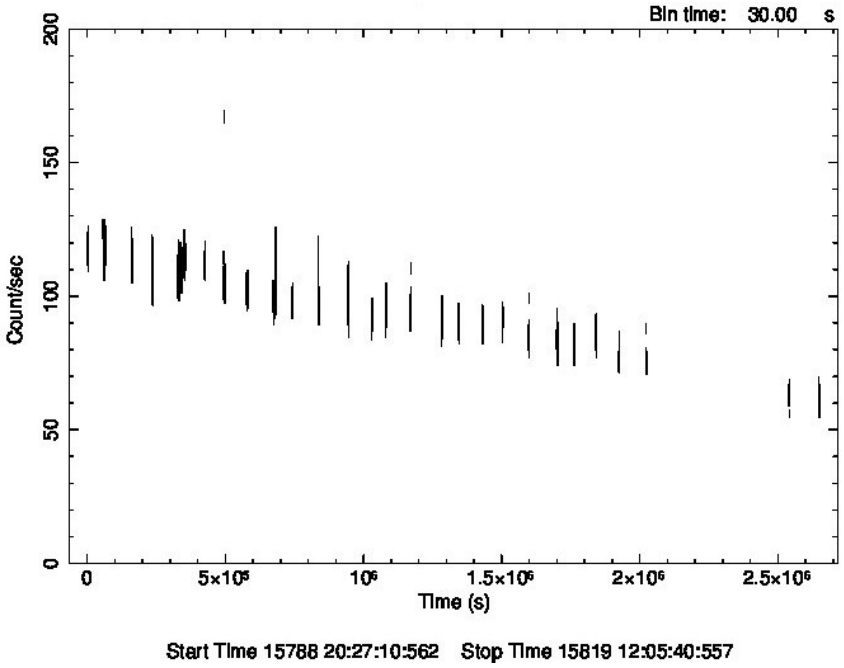

Figure 2.13: 2011 outburst Lightcurve of IGR J17498-2921. Plot is given in count per second vs. time in seconds. The lightcurve extracted from Standard 2f data mode.

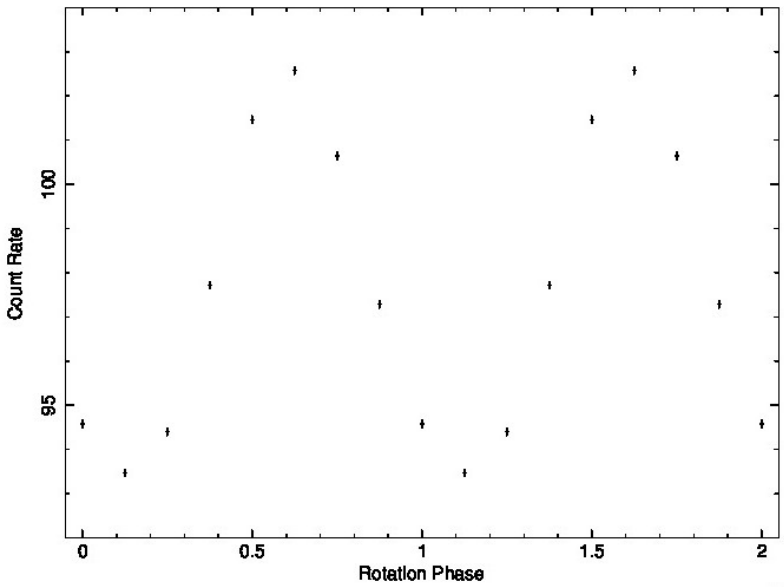

Figure 2.14: Total pulse of IGR J17498-2921 during 2011 outburst. Pulse is extracted from all data used for the phase-resolved analysis. Plot is given in count rate vs. rotation phase which represents twice rotation. In the x-axis, rotation phase is equals to 1 when the source rotated 360^o and pulse is plotted with 2 rotation phase.

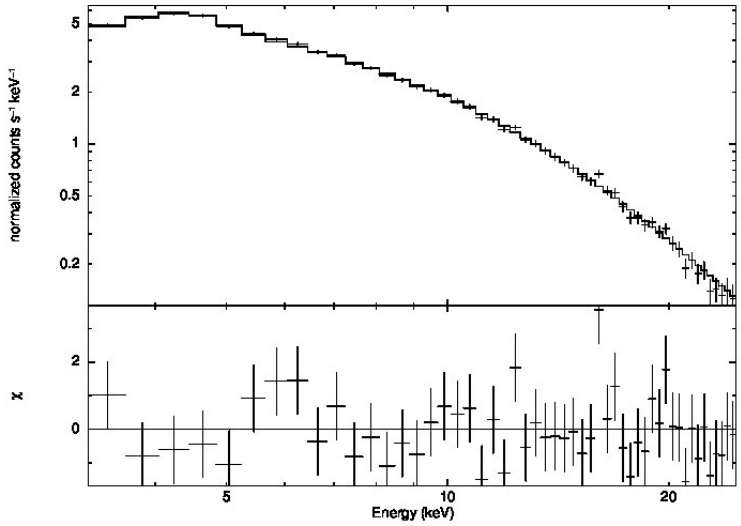

Figure 2.15: Total spectrum of IGR J17498-2921 during 2011 outburst. Spectrum is extracted from all data in Good Xenon mode which are also used in phase-resolved spectroscopy. Spectrum fitted well with blackbody + power law models and nH is fixed at 1.2×10^{22} cm^{-2}, blackbody temperature is found about 1.5 keV and photon index is found about 1.8 .

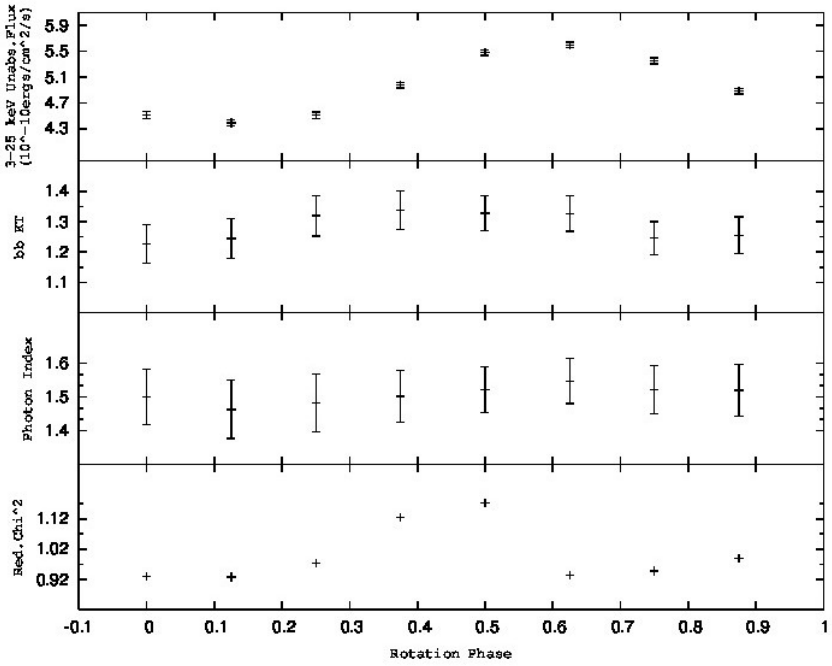

Figure 2.16: Results of Pulse Phase-Spectroscopy of IGR J17498-2921 during 2011 outburst. Y-axis of the first panel is flux in 10^{-10} erg per cm^2 s^{-1}, y-axis of the second panel is blackbody temperature in keV, y-axis of the third panel is photon index and y-axis of the fourth panel is reduced chi^2. X-axis of all panels are rotation phase and the source is divided into 8 rotational phases for the analysis.

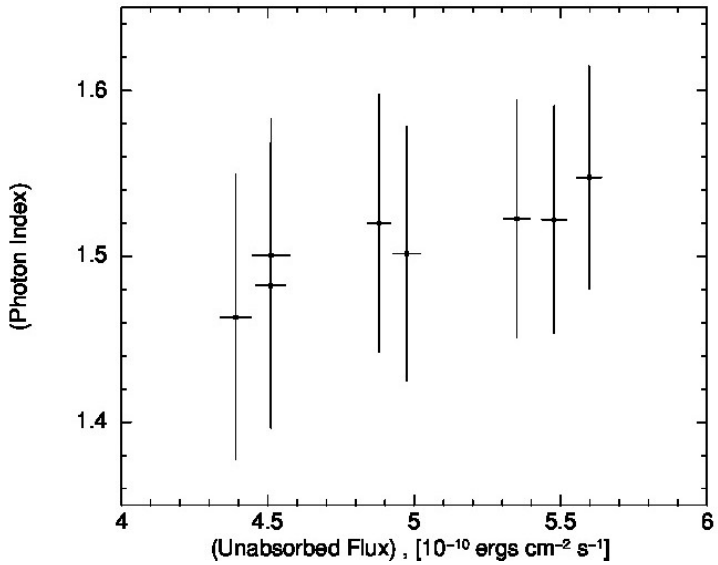

Figure 2.17: Flux vs. Photon Index plot of IGR J17498-2921 during 2011 outburst. With Pearson correlation calculations blackbody temperature, flux and photon index parameters are compared with each other and positive correlation between flux and photon index is found for the source.

Table 2.3: Correlation Table of IGR J17498-2921 during 2011 outburst

	Flux-Blackbody	Flux-Photon Index	Blackbody-Photon Index
Pearson Correlation	.425	.889**	.276
Sig.(2-tailed)	.253	.003	.508
N	8	8	8

** Correlation is significant at the 0.01 level (2-tailed)

2.6 Phase Resolved Spectroscopy of XTE J1807-294

XTE J1807-294 is discovered on February 21, 2003 Markwardt [2003]. Its spin frequency is 191 Hz and its orbital period is 40.1 min with shortest orbital period in all AMSPs Markwardt [2003]. Its companion mass is higher than 0.006 M_s and companion type is a C/O or He WD Patruno [2012].

XTE J1807-294 has showed only one outburst in 2003 February and it lasted about 150 days and pulsations are 90 days of the observations Chou [2008].

In the analysis of XTE J1807-294 in 2003 outburst, about 150 days RXTE observation

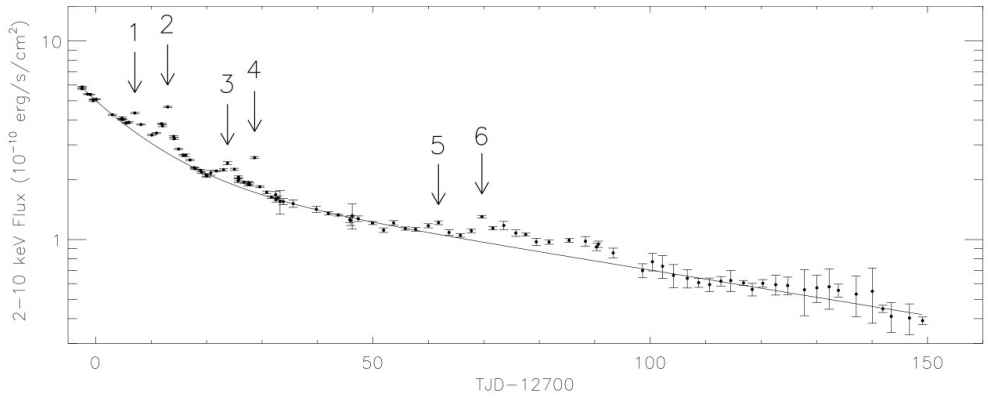

Figure 2.18: Lightcurve of XTE J1807-294 during 2003 outburst with flares Chou [2008]. 1, 2, 3, 4, 5, 6 are flares that occurred during the outburst. Source is divided into 7 states as defined in Chou [2008]. First non-flare state: from beginning of the data to flare 1, first flare state: flare 1 and 2 part , second non-flare state: from flare 2 to flare 3, second flare state: flare 3 and 4 part, third non-flare state: from flare 4 to flare 5, third flare state: flare 5 and 6 part, fourth non-flare state: from flare 4 to the end of the data.

data is divided into 7 states, which consist of 3 flare and 4 non-flare states as defined in Chou [2008]. In Figure 2.18 below, 1, 2, 3, 4, 5, 6 refers to flares occurred during 2003 outburst.

The states are defined in Chou [2008] with respect to flares and non-flare parts. First non-flare state is the part between beginning of the outburst and beginning of the first flare. First flare state is the part covers flare 1 and 2. Second non-flare state is the non-flare part between flare 2 and flare 3. Second flare state is the part covers flare 3 and 4. Third non-flare state is the non-flare part between flare 4 and 5. Third flare state is the part covers flare 5 and 6. Fourth non-flare state is the part between end of flare 6 and end of the outburst. Start and stop dates of the states can be found below in Table 2.4

Observation Ids used in the analysis can be found in Appendix B.

Total pulse obtained from all data and total lightcurve of the source can be seen in Figure 2.19 and Figure 2.20 respectively.

Position of the source is used as R.A : 18^h 06^m 59^s.80 and DEC. : -29^o 24' 30" Markwardt [2003] for the analysis and timing parameters of the system is used as

Table 2.4: States Table of XTE J1807-294 during 2003 outburst

State	Start Date	Stop Date
First Non-Flare	2003-02-28 12:55:16	2003-03-01 23:32:28
First Flare	2003-03-04 22:45:01.2	2003-03-18 23:06:57
Second Non-Flare	2003-03-19 17:58:22.4	2003-03-21 22:06:46.4
Second Flare	2003-03-22 00:03:22.2	2003-04-01 18:36:57
Third Non-Flare	2003-04-02 15:04:52.9	2003-04-28 14:43:58.4
Third Flare	2003-04-30 22:02:07.3	2003-05-18 11:13:23.2
Fourth Non-Flare	2003-05-20 09:00:51.8	2003-06-22 17:20:00.7

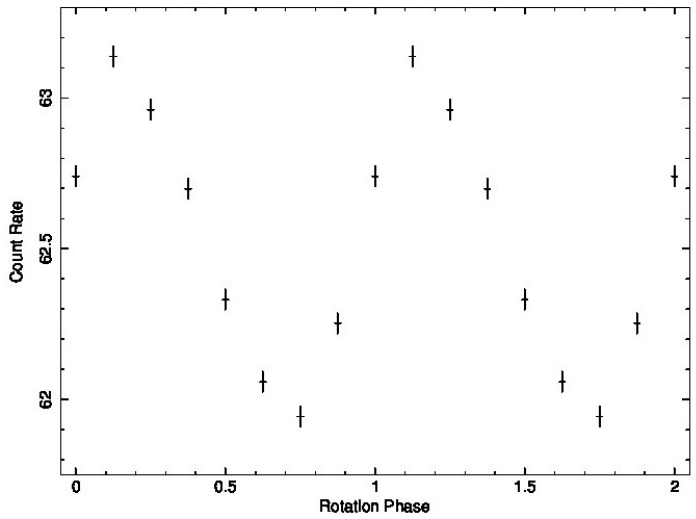

Figure 2.19: Total pulse of XTE J1807-294 during 2003 outburst. Pulse is extracted from all data including 7 states which are used for the phase-resolved analysis. Plot is given in count rate vs. rotation phase which represents twice rotation. In the x-axis, rotation phase is equals to 1 when the source rotated 360^o and pulse is plotted with 2 rotation phase.

orbital period P_{orb} : 2404.41665(s) , spin period P_s : 190.62350702(Hz) , projected semimajor axis $a_x$sini 4.819(light-ms) and epoch of spin frequency t_0 : 52698.5(MJD) Papitto [2011b].

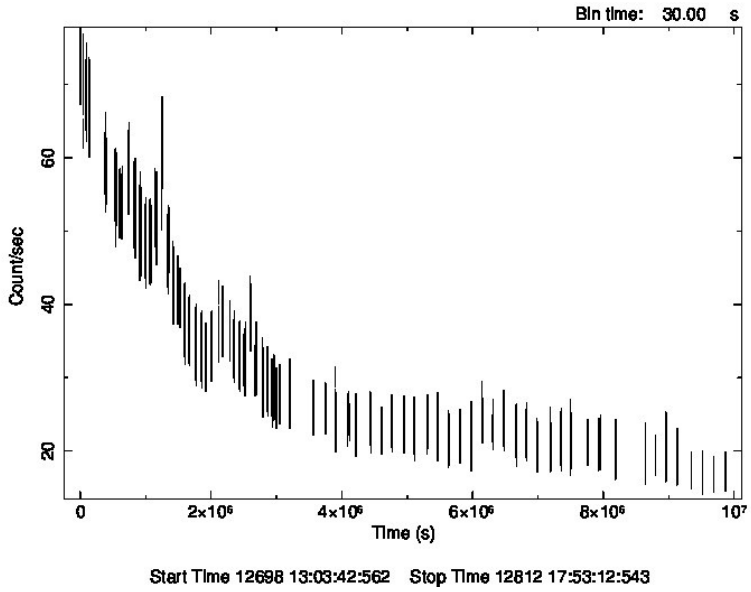

Figure 2.20: Total Lightcurve of XTE J1807-294 during 2003 outburst. Plot is given in count per second vs. time in seconds. The lightcurve extracted from Standard 2f data mode.

2.6.1 First Non-Flare State Analysis of XTE J1807-294

Total pulse obtained from the first non-flare state analysis is shown in Fig 2.21

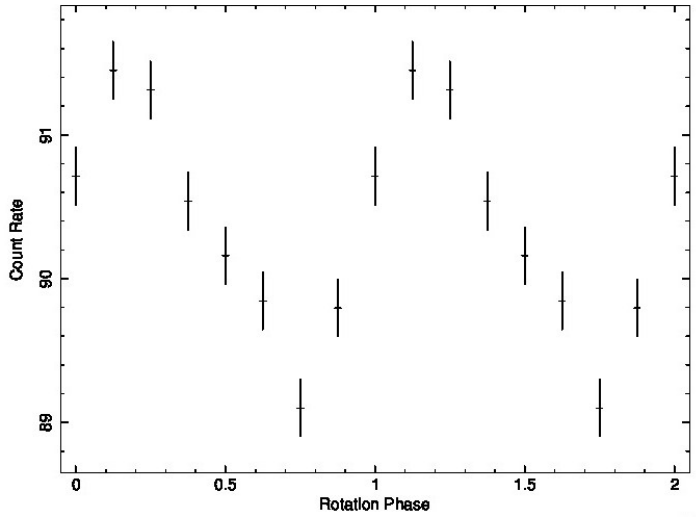

Figure 2.21: Total pulse of XTE J1807-294 in the first Non-Flare State during 2003 outburst. Pulse is extracted from all data used for the first non-flare state phase-resolved analysis. Plot is given in count rate vs. rotation phase which represents twice rotation. In the x-axis, rotation phase is equals to 1 when the source rotated 360^o and pulse is plotted with 2 rotation phase.

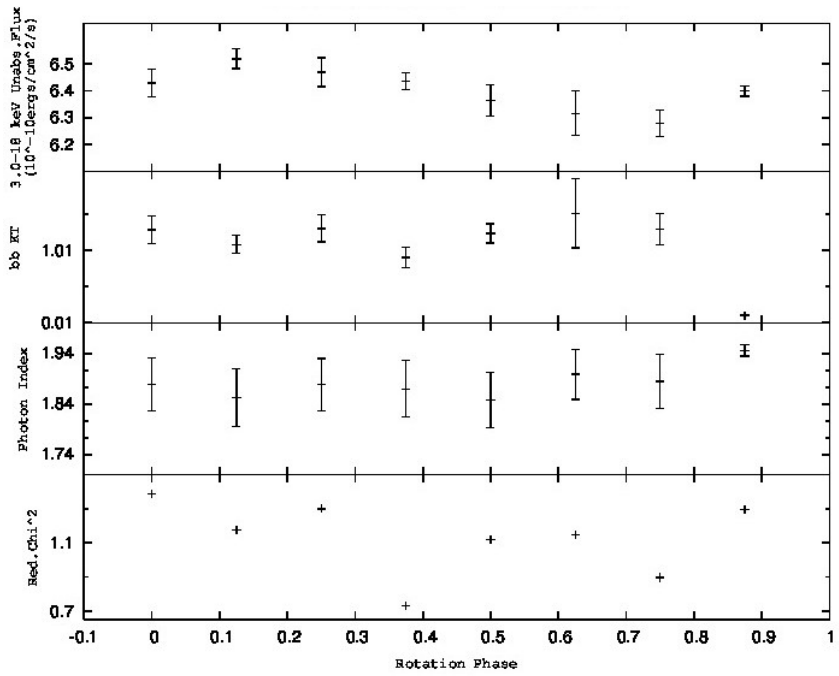

Figure 2.22: The First Non-Flare State Pulse Phase-Spectroscopy Results of XTE J1807-294 during 2003 outburst. Y-axis of the first panel is flux in 10^{-10} erg per cm^2 s^{-1}, y-axis of the second panel is blackbody temperature in keV, y-axis of the third panel is photon index and y-axis of the fourth panel is reduced chi^2. X-axis of all panels are rotation phase and the source is divided into 8 rotational phases for the analysis.

Results of pulse phase resolved x-ray spectroscopy of XTE J1807-294 for the first non-flare state is given in Figure 2.22

In the results of the first non-flare state phase resolved spectroscopy analysis of XTE J1807-294 during 2003 outburst, significant relation between blackbody temperature, photon index and flux is not found. Pearson coefficient values are calculated from average values of each parameter. Results of Pearson correlation coefficient calculations are given in the table below in Table 2.5. All phase spectra can be found in

Table 2.5: Correlation Table of XTE J1807-294 during 2003 outburst in the First Non-Flare State

	Flux-Blackbody	Flux-Photon Index	Blackbody-Photon Index
Pearson Correlation	-.212	-.284	-.637
Sig.(2-tailed)	.615	.496	.089
N	8	8	8

Appendix A section.

2.6.2 First Flare State Analysis of XTE J1807-294

Total pulse obtained from the first flare state analysis is shown in Fig 2.23

Results of pulse phase resolved x-ray spectroscopy of XTE J1807-294 for the first flare state is given in Figure 2.24

In the results of the first flare state phase resolved spectroscopy analysis of XTE J1807-294 during 2003 outburst, negative correlation is found between blackbody temperature and photon index at the rate of -0.895 Pearson correlation constant. Pearson coefficient values are calculated from average values of each parameter. Results of Pearson correlation coefficient calculations are given below in Table 2.6. Blackbody temperature vs. photon index graphic is given below in Figure 2.25. All phase spectra can be found in Appendix A section.

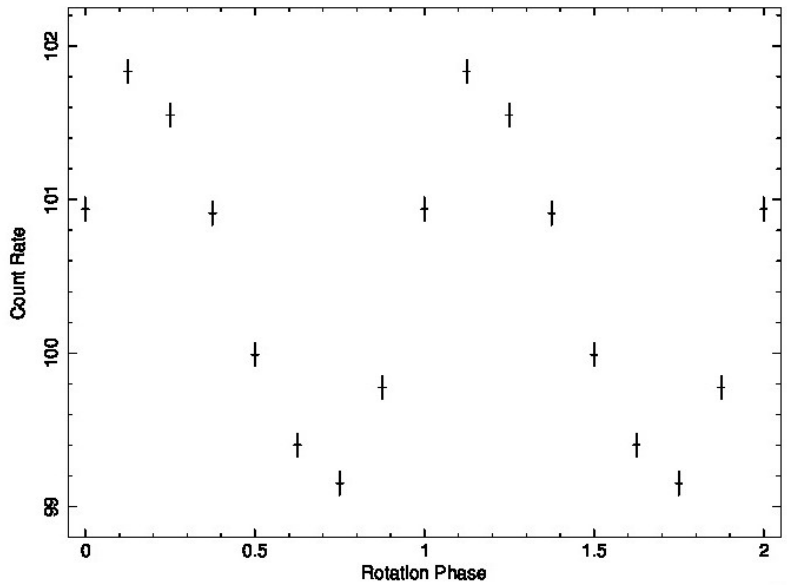

Figure 2.23: Total pulse of XTE J1807-294 in the First Flare State during 2003 outburst. Pulse is extracted from all data used for the first flare state phase-resolved analysis. Plot is given in count rate vs. rotation phase which represents twice rotation. In the x-axis, rotation phase is equals to 1 when the source rotated 360^o and pulse is plotted with 2 rotation phase.

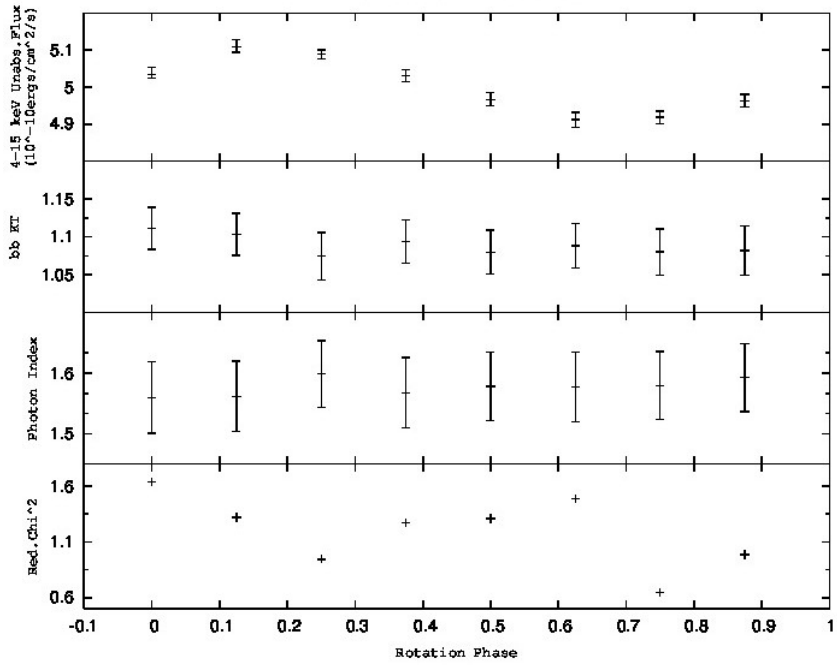

Figure 2.24: The First Flare State Pulse Phase-Spectroscopy Results of XTE J1807-294 during 2003 outburst. Y-axis of the first panel is flux in 10^{-10} erg per cm^2 s^{-1}, y-axis of the second panel is blackbody temperature in keV, y-axis of the third panel is photon index and y-axis of the fourth panel is reduced chi^2. X-axis of all panels are rotation phase and the source is divided into 8 rotational phases for the analysis.

Table 2.6: Correlation Table of XTE J1807-294 during 2003 outburst in the First Flare State

	Flux-Blackbody	Flux-Photon Index	Blackbody-Photon Index
Pearson Correlation	.374	-.203	-.895**
Sig.(2-tailed)	.361	.629	.003
N	8	8	8

** Correlation is significant at the 0.01 level (2-tailed)

2.6.3 Second Non-Flare State Analysis of XTE J1807-294

Total pulse obtained from Second non-flare state analysis is shown in Fig 2.26

Results of pulse phase resolved x-ray spectroscopy of XTE J1807-294 for the Second non-flare state is given in Figure 2.27

In the results of Second non-flare state phase resolved spectroscopy analysis of XTE

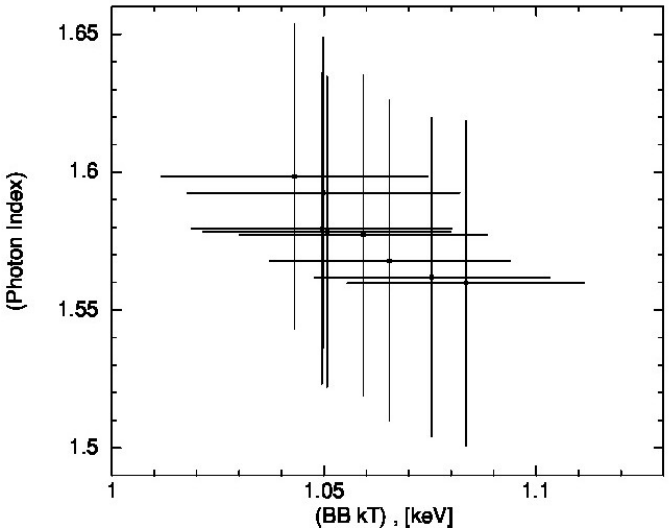

Figure 2.25: Blackbody Temperature vs. Photon Index plot of XTE J1807-294 during 2003 outburst in the First Flare State. With Pearson correlation calculations blackbody temperature, flux and photon index parameters are compared with each other and negative correlation between blackbody temperature and photon index is found for the source.

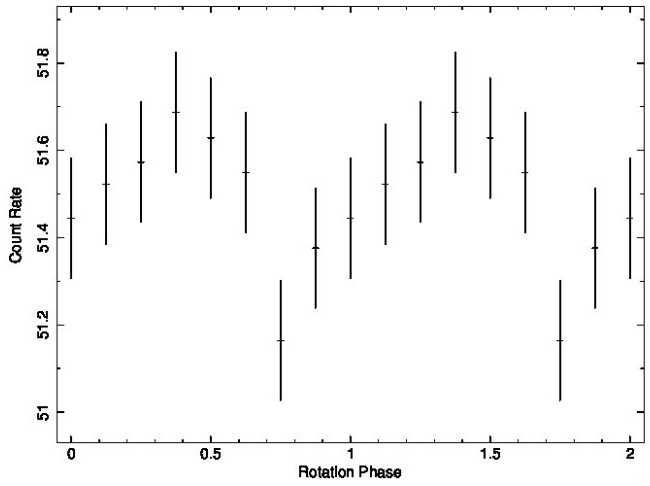

Figure 2.26: Total pulse of XTE J1807-294 in Second Non-Flare State during 2003 outburst. Pulse is extracted from all data used for the second non-flare state phase-resolved analysis. Plot is given in count rate vs. rotation phase which represents twice rotation. In the x-axis, rotation phase is equals to 1 when the source rotated 360^o and pulse is plotted with 2 rotation phase.

J1807-294 during 2003 outburst, positive correlation is found between flux and photon index at the rate of 0.738 Pearson correlation constant. Pearson coefficient values are calculated from average values of each parameter. Results of Pearson correlation

Table 2.7: Correlation Table of XTE J1807-294 during 2003 outburst in the Second Non-Flare State

	Flux-Blackbody	Flux-Photon Index	Blackbody-Photon Index
Pearson Correlation	.213	.738*	-.551
Sig.(2-tailed)	.613	.036	.157
N	8	8	8

** Correlation is significant at the 0.01 level (2-tailed)

coefficient calculations are given below in Table 2.7. Flux vs. photon index plot is given below in Figure 2.28. All phase spectra can be found in Appendix A section.

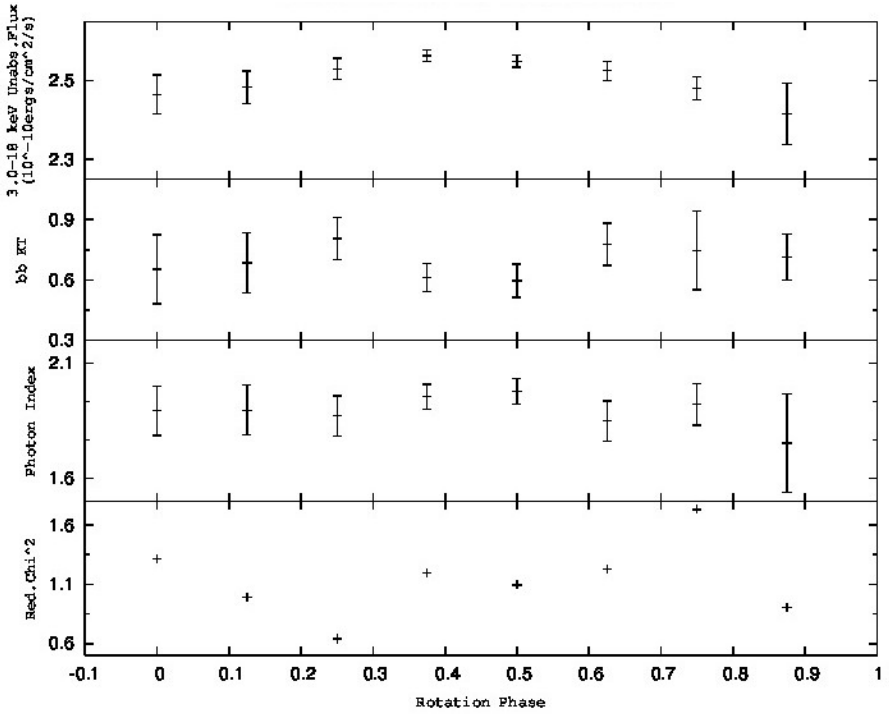

Figure 2.27: Second Non-Flare State Pulse Phase-Spectroscopy Results of XTE J1807-294 during 2003 outburst. Y-axis of the first panel is flux in 10^{-10} erg per cm^2 s^{-1}, y-axis of the second panel is blackbody temperature in keV, y-axis of the third panel is photon index and y-axis of the fourth panel is reduced chi^2. X-axis of all panels are rotation phase and the source is divided into 8 rotational phases for the analysis.

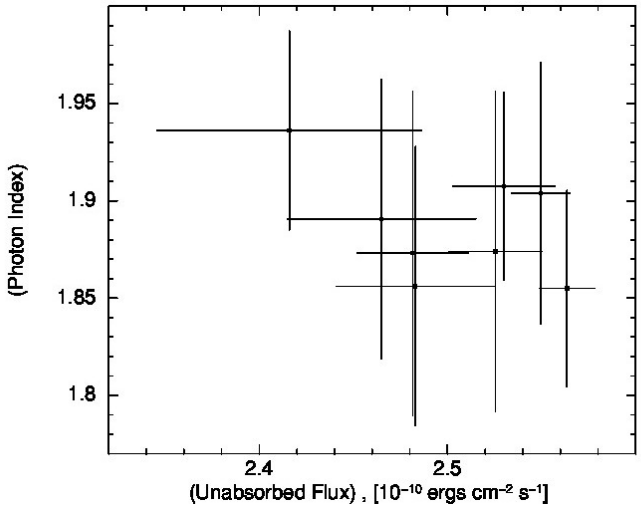

Figure 2.28: Flux vs. Photon Index plot of XTE J1807-294 during 2003 outburst in Second Non-Flare State

2.6.4 Second Flare State Analysis of XTE J1807-294

Total pulse obtained from Second flare state analysis is shown in Fig 2.29

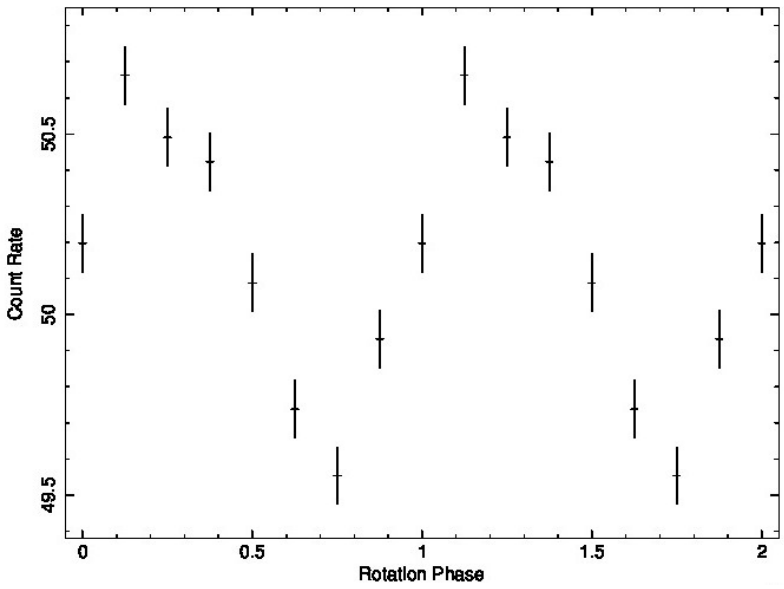

Figure 2.29: Total pulse of XTE J1807-294 in Second Flare State during 2003 outburst. Pulse is extracted from all data used for the second flare state phase-resolved analysis. Plot is given in count rate vs. rotation phase which represents twice rotation. In the x-axis, rotation phase is equals to 1 when the source rotated 360^o and pulse is plotted with 2 rotation phase.

Results of pulse phase resolved x-ray spectroscopy of XTE J1807-294 for the Second flare state is given in Figure 2.30

In the results of Second flare state phase resolved spectroscopy analysis of XTE J1807-294 during 2003 outburst, positive correlation is found between blacbody temperature and photon index at the rate of 0.769 Pearson correlation constant. Pearson coefficient values are calculated from average values of each parameter. Results of Pearson correlation coefficient calculations are given below in Table 2.8. Flux vs. photon index plot is given below in Figure 2.31. All phase spectra can be found in Appendix A section.

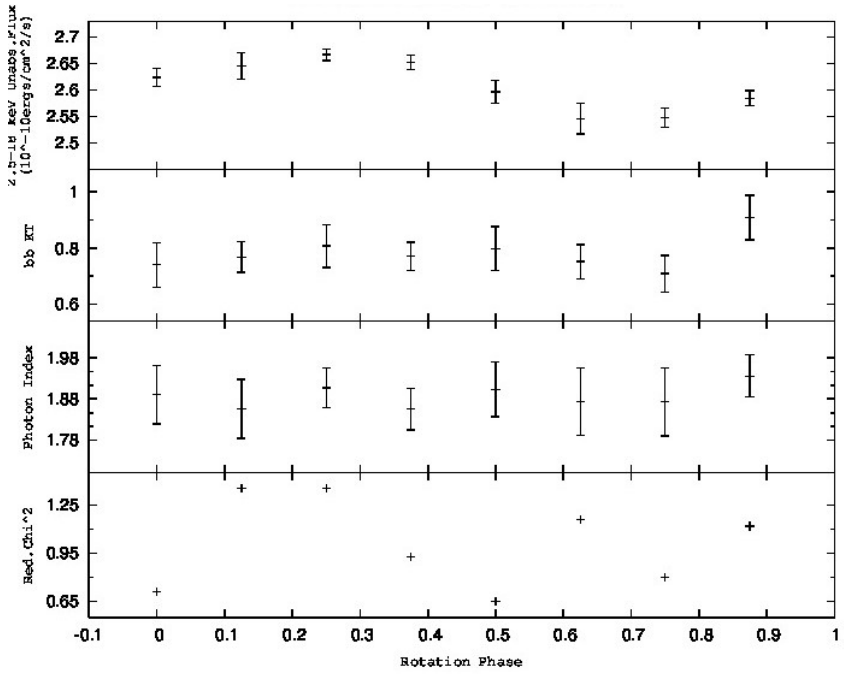

Figure 2.30: Second Flare State Pulse Phase-Spectroscopy Results of XTE J1807-294 during 2003 outburst. Y-axis of the first panel is flux in 10^{-10} erg per cm^2 s^{-1}, y-axis of the second panel is blackbody temperature in keV, y-axis of the third panel is photon index and y-axis of the fourth panel is reduced chi^2. X-axis of all panels are rotation phase and the source is divided into 8 rotational phases for the analysis.

	Flux-Blackbody	Flux-Photon Index	Blackbody-Photon Index
Pearson Correlation	.154	-.108	.769
Sig.(2-tailed)	.717	.799	.026
N	8	8	8

** Correlation is significant at the 0.01 level (2-tailed)

Table 2.8: Correlation Table of XTE J1807-294 during 2003 outburst in the Second Flare State

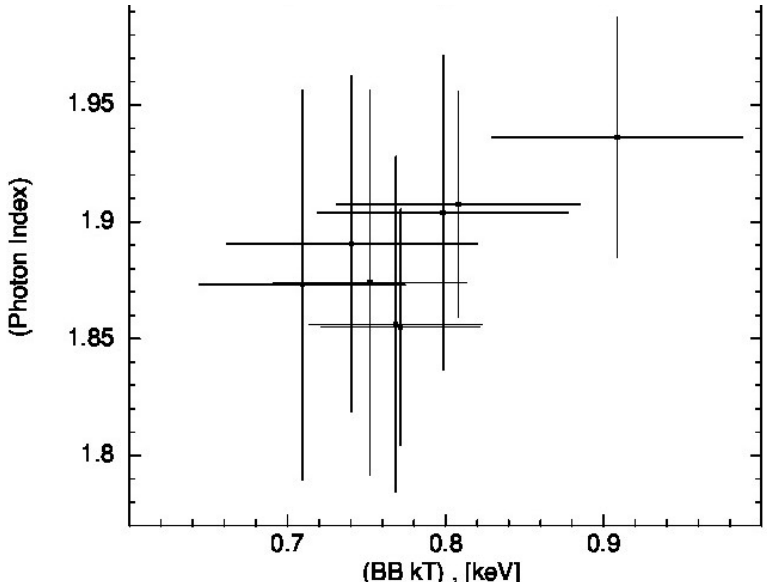

Figure 2.31: Flux vs. Photon Index plot of XTE J1807-294 during 2003 outburst in Second Flare State. With Pearson correlation calculations blackbody temperature, flux and photon index parameters are compared with each other and positive correlation between flux and photon index is found for the source.

2.6.5 Third Non-Flare State Analysis of XTE J1807-294

Total pulse obtained from Third non-flare state analysis is shown in Fig 2.32

Results of pulse phase resolved x-ray spectroscopy of XTE J1807-294 for the Third non-flare state is given in Figure 2.33

In the results of Third non-flare state phase resolved spectroscopy analysis of XTE J1807-294 during 2003 outburst, any significant relation between blackbody temperature, photon index and flux is found. Pearson coefficient values are calculated from average values of each parameter. Results of Pearson correlation coefficient calcu-

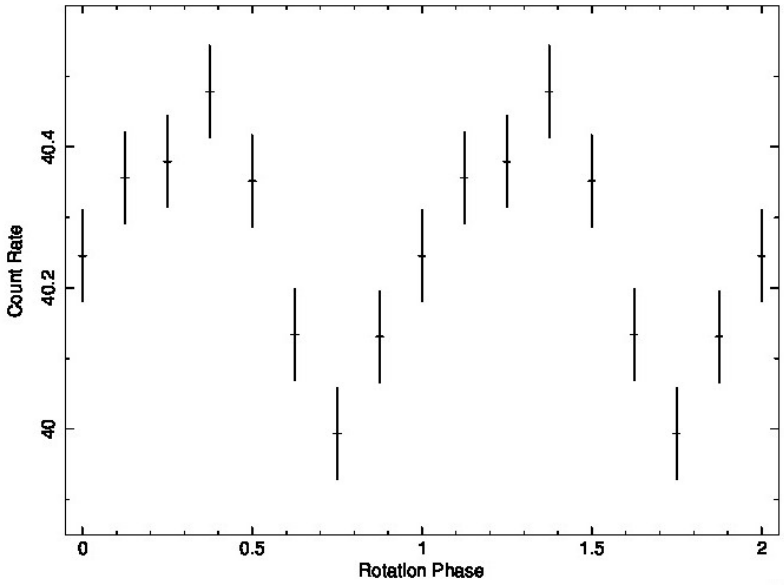

Figure 2.32: Total pulse of XTE J1807-294 in Third Non-Flare State during 2003 outburst. Pulse is extracted from all data used for the third non-flare state phase-resolved analysis. Plot is given in count rate vs. rotation phase which represents twice rotation. In the x-axis, rotation phase is equals to 1 when the source rotated 360^o and pulse is plotted with 2 rotation phase.

Table 2.9: Correlation Table of XTE J1807-294 during 2003 outburst in the Third Non-Flare State

	Flux-Blackbody	Flux-Photon Index	Blackbody-Photon Index
Pearson Correlation	.230	-.108	.091
Sig.(2-tailed)	.584	.800	.830
N	8	8	8

lations are given in the table below in Table 2.9. All phase spectra can be found in Appendix A section.

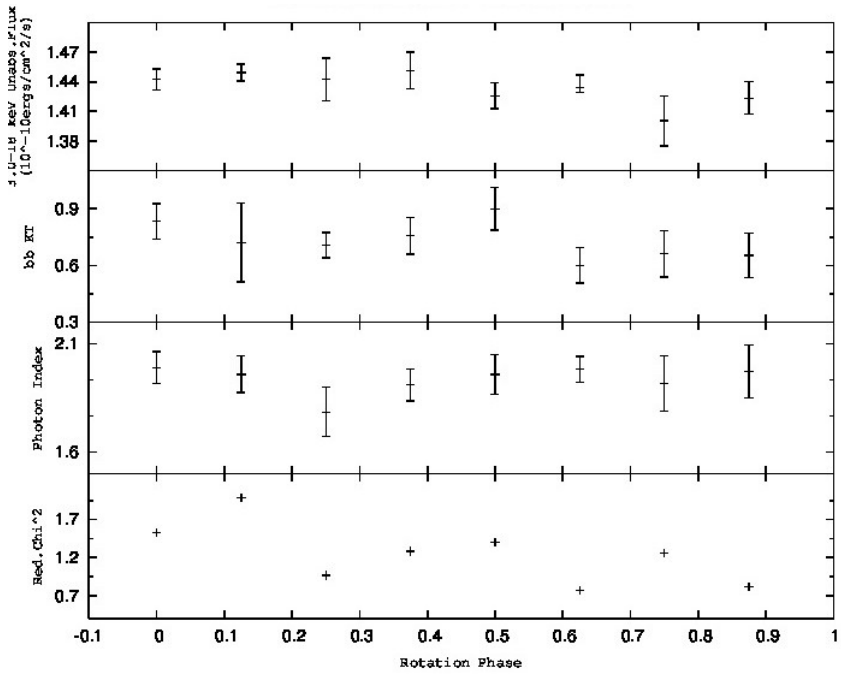

Figure 2.33: Third Non-Flare State Pulse Phase-Spectroscopy Results of XTE J1807-294 during 2003 outburst. Y-axis of the first panel is flux in 10^{-10} erg per cm^2 s^{-1}, y-axis of the second panel is blackbody temperature in keV, y-axis of the third panel is photon index and y-axis of the fourth panel is reduced chi^2. X-axis of all panels are rotation phase and the source is divided into 8 rotational phases for the analysis.

2.6.6 Third Flare State Analysis of XTE J1807-294

Total pulse obtained from Third flare state analysis is shown in Fig 2.34

Results of pulse phase resolved x-ray spectroscopy of XTE J1807-294 for the Third flare state is given in Figure 2.35

In the results of Third flare state phase resolved spectroscopy analysis of XTE J1807-294 during 2003 outburst, any significant relation between blackbody temperature, photon index and flux is found. Pearson coefficient values are calculated from average values of each parameter. Results of Pearson correlation coefficient calculations are given in the table below in Table 2.10. All phase spectra can be found in Appendix A section.

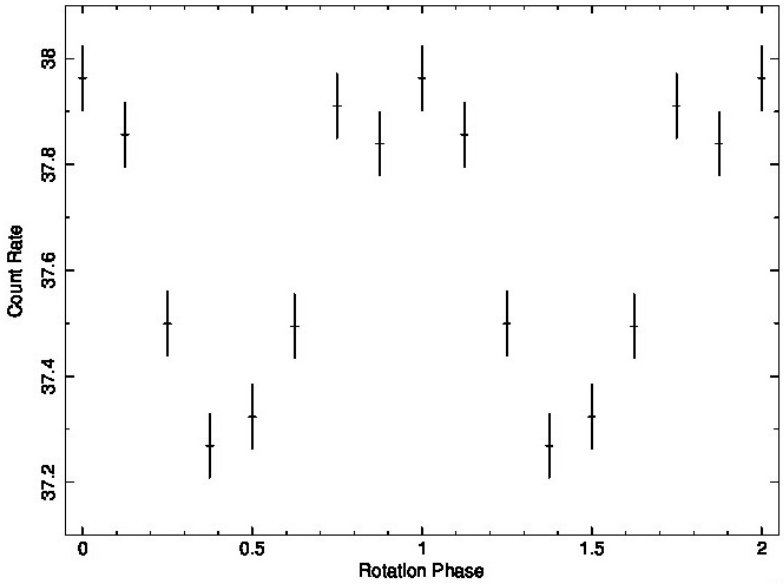

Figure 2.34: Total pulse of XTE J1807-294 in Third Flare State during 2003 outburst. Pulse is extracted from all data used for the third flare state phase-resolved analysis. Plot is given in count rate vs. rotation phase which represents twice rotation. In the x-axis, rotation phase is equals to 1 when the source rotated 360^o and pulse is plotted with 2 rotation phase.

Table 2.10: Correlation Table of XTE J1807-294 during 2003 outburst in the Third Flare State

	Flux-Blackbody	Flux-Photon Index	Blackbody-Photon Index
Pearson Correlation	-.158	.289	-.675
Sig.(2-tailed)	.709	.487	.066
N	8	8	8

2.6.7 Fourth Non-Flare State Analysis of XTE J1807-294

Total pulse obtained from Fourth non-flare state analysis is shown in Fig 2.36

Results of pulse phase resolved x-ray spectroscopy of XTE J1807-294 for the Fourth non-flare state is given in Figure 2.37

In the results of Fourth non-flare state phase resolved spectroscopy analysis of XTE J1807-294 during 2003 outburst, positive correlation is found between flux and photon index at the rate of 0.812 Pearson correlation constant but the total pulse is not sufficient enough for the correlation. Pearson coefficient values are calculated from average values of each parameter. Results of Pearson correlation coefficient calcula-

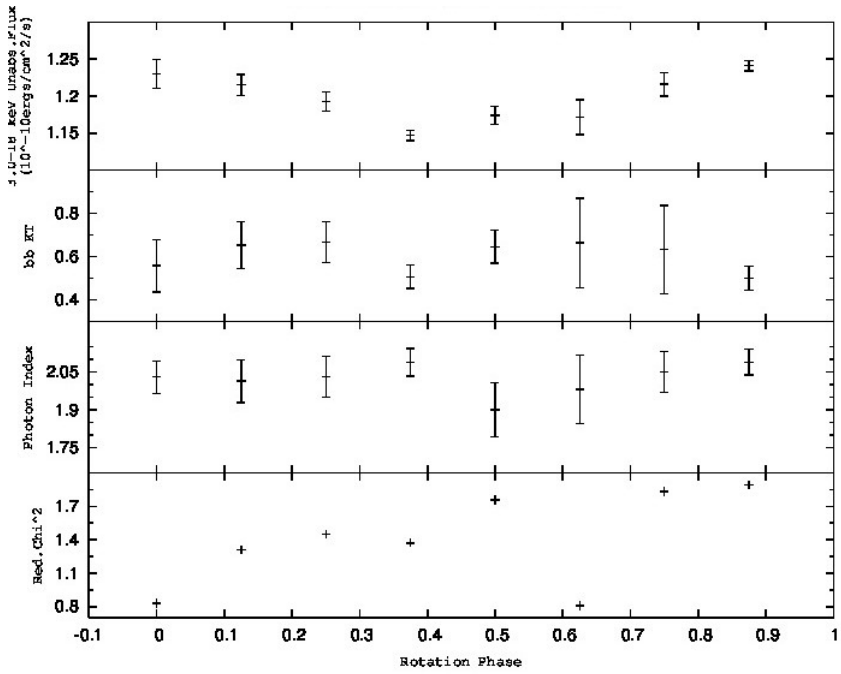

Figure 2.35: Third Flare State Pulse Phase-Spectroscopy Results of XTE J1807-294 during 2003 outburst. Y-axis of the first panel is flux in 10^{-10} erg per cm^2 s^{-1}, y-axis of the second panel is blackbody temperature in keV, y-axis of the third panel is photon index and y-axis of the fourth panel is reduced chi^2. X-axis of all panels are rotation phase and the source is divided into 8 rotational phases for the analysis.

Table 2.11: Correlation Table of XTE J1807-294 during 2003 outburst in the Fourth Non-Flare State

	Flux-Blackbody	Flux-Photon Index	Blackbody-Photon Index
Pearson Correlation	.206	.812*	-.246
Sig.(2-tailed)	.624	.014	.557
N	8	8	8

** Correlation is significant at the 0.05 level (2-tailed)

tions are given below in Table 2.11. All phase spectra can be found in Appendix A section.

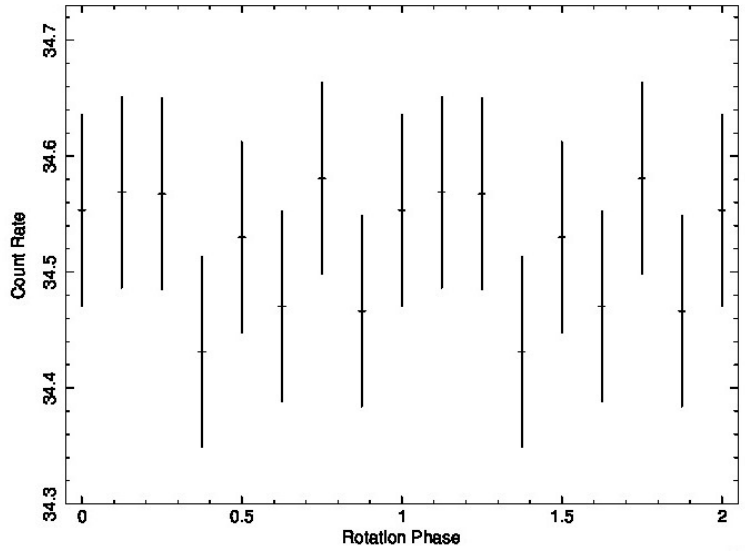

Figure 2.36: Total pulse of XTE J1807-294 in Fourth Non-Flare State during 2003 outburst. Pulse is extracted from all data used for the fourth non-flare state phase-resolved analysis. Plot is given in count rate vs. rotation phase which represents twice rotation. In the x-axis, rotation phase is equals to 1 when the source rotated 360^o and pulse is plotted with 2 rotation phase.

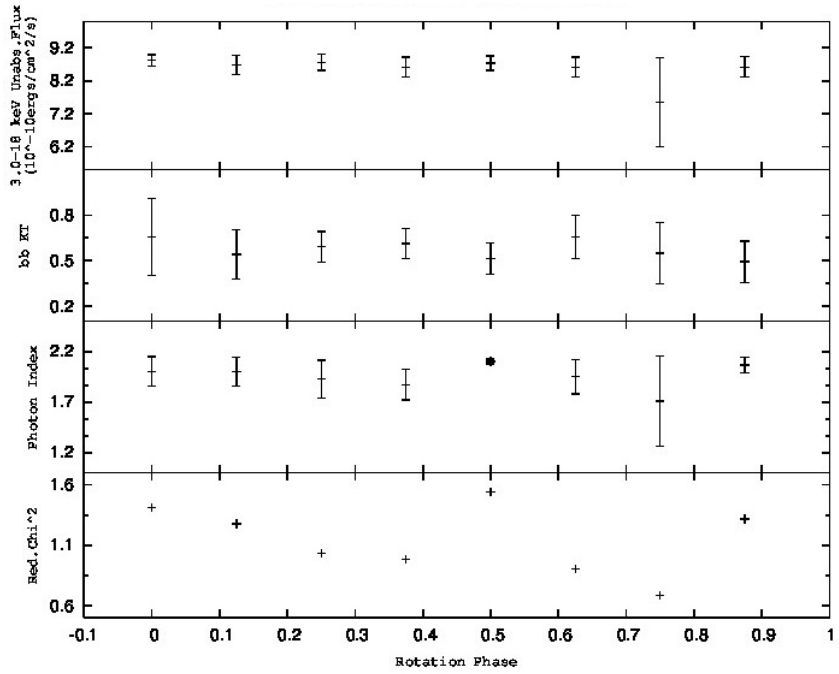

Figure 2.37: Fourth Non-Flare State Pulse Phase-Spectroscopy Results of XTE J1807-294 during 2003 outburst. Y-axis of the first panel is flux in 10^{-10} erg per cm^2 s^{-1}, y-axis of the second panel is blackbody temperature in keV, y-axis of the third panel is photon index and y-axis of the fourth panel is reduced chi^2. X-axis of all panels are rotation phase and the source is divided into 8 rotational phases for the analysis.

CHAPTER 3

CONCLUSION

In this study, pulse phase resolved X-ray spectroscopy of four accretion powered millisecond pulsars which are IGR J00291+5934 , IGR J17498-2921 , XTE J0929-314 and XTE J1807-294 is presented for the first time. Phase dependent changes during their outbursts are checked for possible correlations of spectral parameters such as photon index and blackbody temperature with rotation phase using archive of Rossi X-ray Timing Explorer (RXTE) observations.

In the RXTE/PCA Good Xenon data mode phase resolved x-ray spectroscopy between 3-18keV analysis of IGR J00291+5934 Eckert [2004] in September 2008 outburst, significant relation between blackbody temperature, photon index and flux is not found.

In the phase resolved x-ray spectroscopy analysis of IGR J17498-2921 Gibaud [2011] for RXTE/PCA Good Xenon data mode between 3-25keV energy range in 2011 outburst, positive correlation is found between photon index and flux at the rate of 0.899 Pearson correlation constant. Increase in accretion rate causes to more softer emitted spectra which could be indication of radiation perpendicular to accretion column. When the accretion column becomes more optically thick, radiation escaping perpendicular to the accretion column becomes softer which might be the reason of positive correlation between flux and photon index for the source.

Lastly, in the analysis of XTE J1807-294 Markwardt [2003] in 2003 outburst, about 150 days RXTE observation data is divided into 7 states, which consist of 3 flare and 4 non-flare states. In the /PCA Good Xenon data mode phase resolved x-ray

spectroscopy analysis between 3-18keV energy range for first non-flare, third non-flare state, third flare state and fourth non-flare state, correlations between blackbody temperature, photon index and flux are not found.

On the other hand, in the first flare state RXTE/PCA Good Xenon data mode phase resolved x-ray spectroscopy between 4-15keV analysis, negative correlation is found between blackbody temperature and photon index at the rate of -0.895 Pearson correlation constant. In the Second flare state RXTE/PCA Good Xenon data mode phase resolved x-ray spectroscopy between 2.5-18keV analysis, positive correlation is found between blackbody temperature and photon index at the rate of 0.769 Pearson correlation constant. In the Second non-flare state RXTE/PCA Good Xenon data mode phase resolved x-ray spectroscopy between 3-18keV analysis, positive correlation is found between flux and photon index at the rate of 0.738 Pearson correlation constant. Negative correlation in first flare state and negative correlation in second flare and second non-flare state might be related with pulse average flux. When the pulse average flux is higher, total accretion rate is higher and source becomes harder with increase in blackbody temperature which might be the cause of negative correlation between blackbody temperature and photon index for the first flare state. On the contrary, when the pulse average flux is lower, total accretion rate is lower and the source becomes softer with increasing blackbody temperature which might be the cause of positive correlation between the parameters for the second flare and second non-flare state.

In the RXTE/PCA Good Xenon data mode phase resolved x-ray spectroscopy between 3-18keV analysis of XTE J0929-314 Remillard [2002] in 2002 outburst, negative correlation is found between photon index and blackbody temperature at the rate of -0.938 Pearson correlation constant. Negative correlation between the parameters for the analysis of XTE J0929-314 might be caused by the similar reason as for first flare state of XTE J1807-294. With the increase in total accretion rate, the source becomes harder with increase in blackbody temperature and as a result of this negative correlation has been observed between photon index and blackbody temperature. For all sources, correlation Table 3.1 is given below for the sources which have showed correlation between the parameters.

Table 3.1: Correlations Between Parameters Table of the Sources

Source		Flux - BB temp	Flux - Ph.ind	BB temp - Ph.ind
IGR J17498-2921		No	Positive	No
XTE J0929-314		No	No	Negative
XTE J1807-294	first flare	No	No	Negative
XTE J1807-294	second flare	No	No	Positive
XTE J1807-294	second non-flare	No	No	Positive

REFERENCES

A. Alpar. A new class of radio pulsars-back in 1982. *AIP Conference Proceedings*, 1068:3–8, 2008.

Y. Chou. Precise orbital parameters and anomalous phase variations of the accretion-powered millisecond pulsar xte j1807-294. *The Astrophysics Journal*, 678(2): 1316–1323, 2008.

D. Eckert. Igr j00291+5934, a new x-ray transient discovered with integral. *The Astronomer's Telegram*, (352), 2004.

M. Falanga. Spectral and timing properties of the accreting x-ray millisecond pulsar igr j17498–2921. *Astronomy and Astrophysics*, 545(id.A26):9, 2012.

A. Fowler. *Nucleosynthesis in massive stars and supernovae*. University of Chicago Press, 1965.

D. Galloway. Discovery of a high-latitude accreting millisecond pulsar in an ultra-compact binary. *The Astrophysical Journal*, 576(2):L137–L140, 2002.

L. Gibaud. A new hard x-ray transient discovered by integral: Igrj17498-2921. *The Astronomer's Telegram*, (3551), 2011.

A. Giles. The optical counterpart of xte j0929-314: the third transient millisecond x-ray pulsar. *MNRAS*, 361(4):1180–1186, 2005.

A. Lecompte.

D. Lorimer. Binary and millisecond pulsars. *Living Reviews in Relativity*, 11(8), 2008. URL `http://www.livingreviews.org/lrr-2008-8`.

C. Markwardt. Discovery of a fourth accreting millisecond pulsar, xte j1807-294. *The Astronomer's Telegram*, (122), 2003.

A. Papitto. Spin down during quiescence of the fastest known accretion-powered pulsar. *Astronomy and Astrophysics*, 528(id.A55):6, 2011a.

A. Papitto. Integral and rxte observations of accreting millisecond pulsar igr j00291+5954 in outburst. *Astronomy and Astrophysics*, 535(id.L4):4, 2011b.

A. Patruno. Accreting millisecond x-ray pulsars. *ArXiv*, 1206.2727v1, 2012.

R. Remillard. Xte j0929-314. *IAU Circ.*, (7888,2), 2002.

H. Schatz. End point of the rp process on accreting neutron stars. *Physical Review Letters*, 86(16):3471 – 3474, 2001.

G. Srinivasan. Recycled pulsars. *New Astronomy Reviews*, 54(3-6):93 – 100, 2010.

T. Strohmayer. *"New Views of Thermonuclear Bursts" in Compact stellar X-ray sources*. Cambridge University Press, 2006.

A. Torres. Observations of the 599 hz accreting x-ray pulsar igr j00291+5934 during the 2004 outburst and in quiescence. *The Astrophysical Journal*, 672(2):1079–1090, 2008.

A. Watts. Thermonuclear burs oscillations. *Ann.Rev.Astron.Astrophys*, 50:609 – 640, 2012.

APPENDIX A

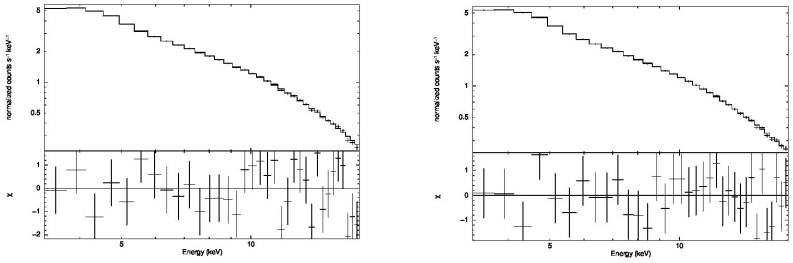

(a) First phase spectrum

(b) Second phase spectrum

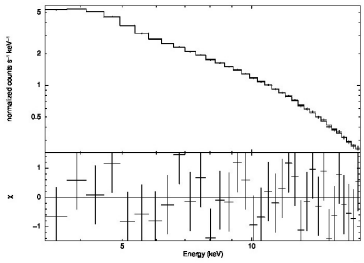

(c) Third phase spectrum

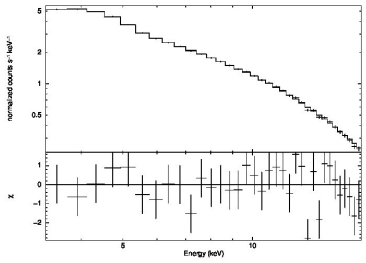

(d) Fourth phase spectrum

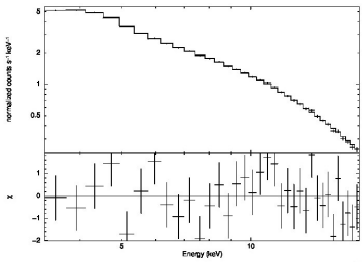

(e) Fifth phase spectrum

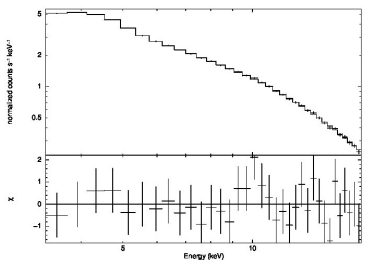

(f) Sixth phase spectrum

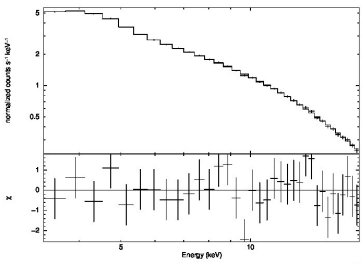

(g) Seventh phase spectrum

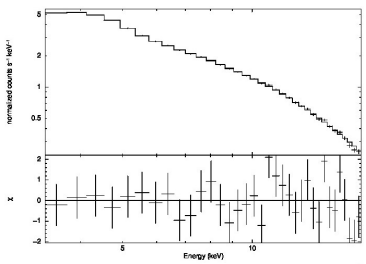

(h) Eighth phase spectrum

Figure A.1: Phase Spectra of XTE J0929-314 in 2003 Outburst

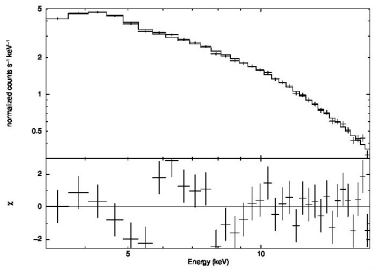

(a) First phase spectrum

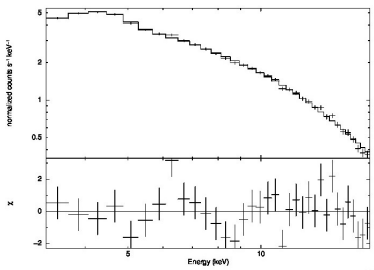

(b) Second phase spectrum

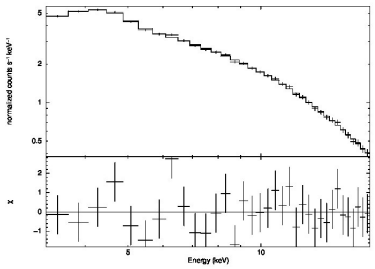

(c) Third phase spectrum

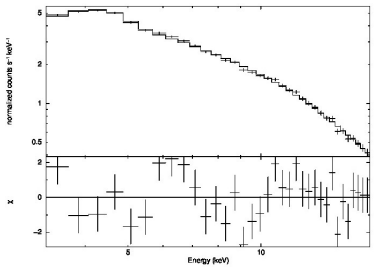

(d) Fourth phase spectrum

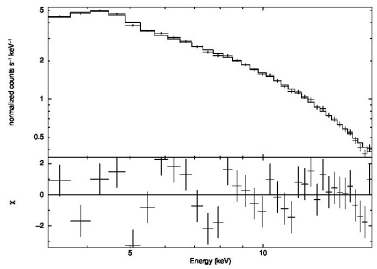

(e) Fifth phase spectrum

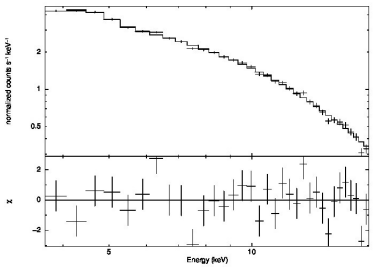

(f) Sixth phase spectrum

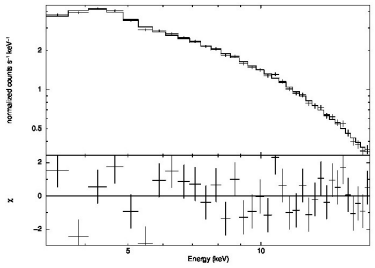

(g) Seventh phase spectrum

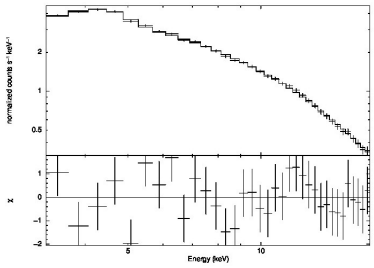

(h) Eighth phase spectrum

Figure A.2: Phase Spectra of IGR J00291+5954 in 2008 September outburst

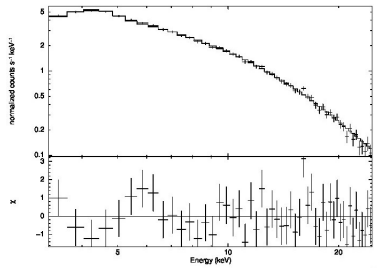

(a) First phase spectrum

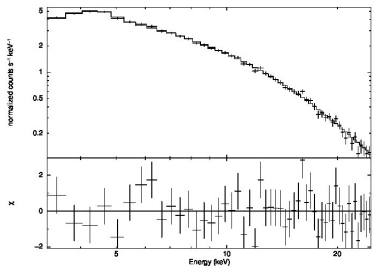

(b) Second phase spectrum

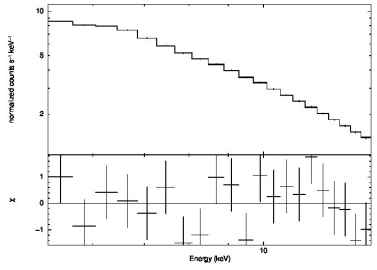

(c) Third phase spectrum

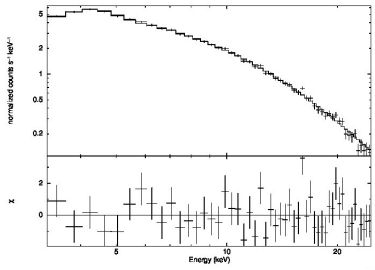

(d) Fourth phase spectrum

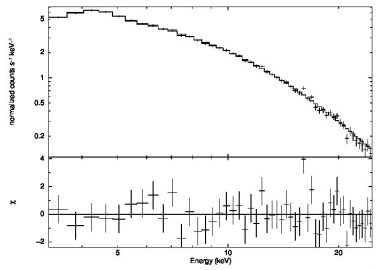

(e) Fifth phase spectrum

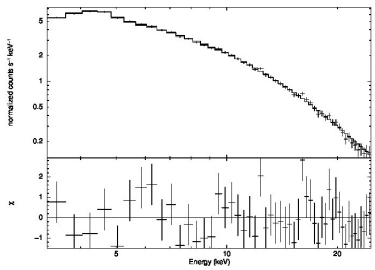

(f) Sixth phase spectrum

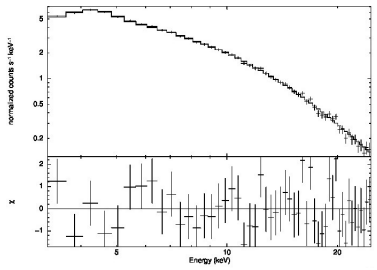

(g) Seventh phase spectrum

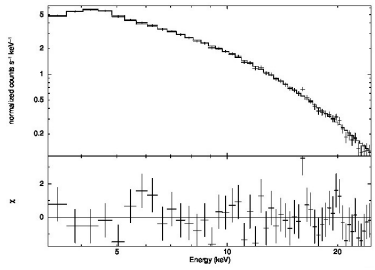

(h) Eighth phase spectrum

Figure A.3: Phase Spectra of IGR J17498-2921 during 2011 outburst

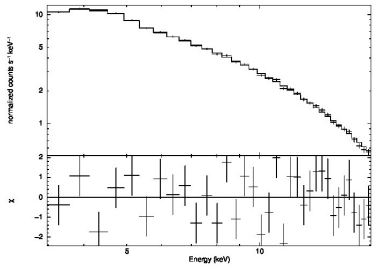

(a) First phase spectrum

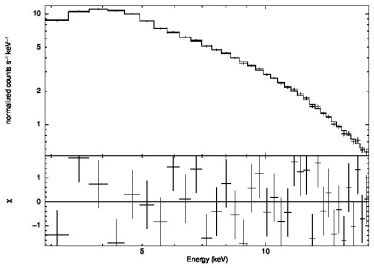

(b) Second phase spectrum

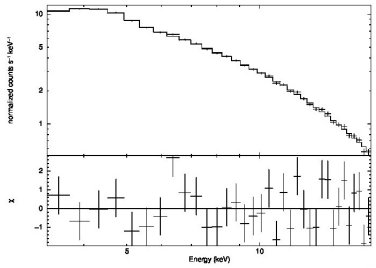

(c) Third phase spectrum

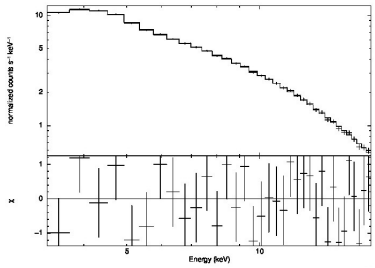

(d) Fourth phase spectrum

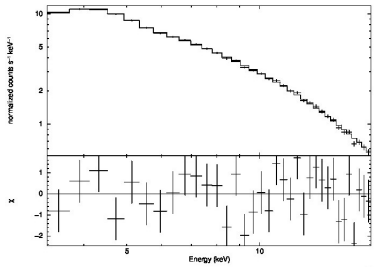

(e) Fifth phase spectrum

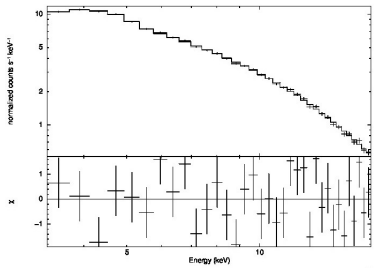

(f) Sixth phase spectrum

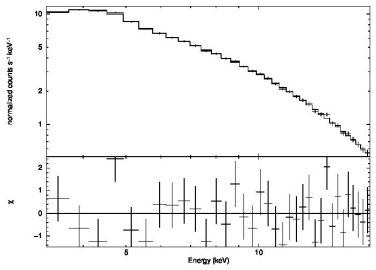

(g) Seventh phase spectrum

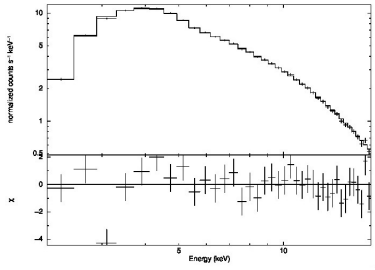

(h) Eighth phase spectrum

Figure A.4: Phase Spectra of XTE J1807-294 in First Non-Flare State

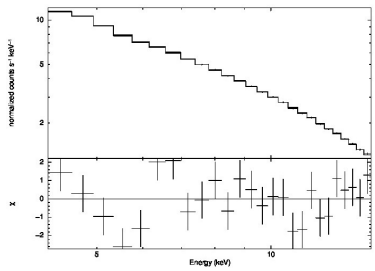

(a) First phase spectrum

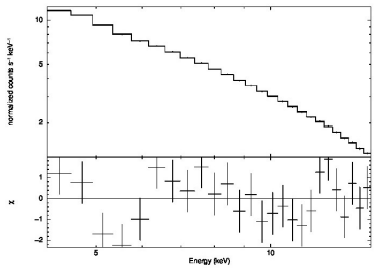

(b) Second phase spectrum

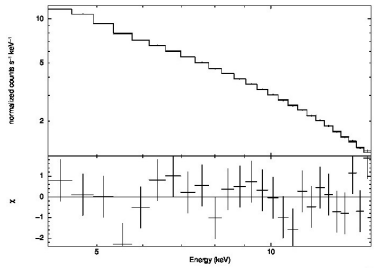

(c) Third phase spectrum

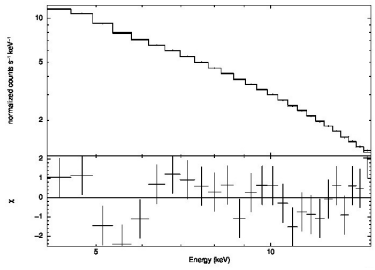

(d) Fourth phase spectrum

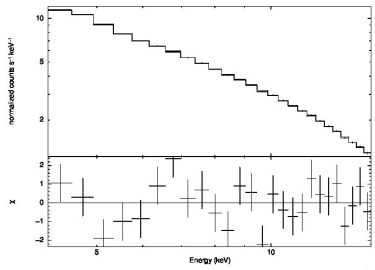

(e) Fifth phase spectrum

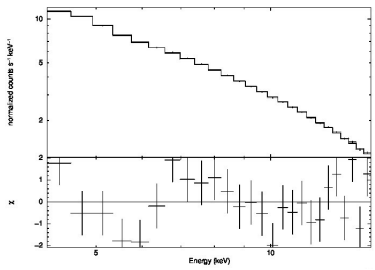

(f) Sixth phase spectrum

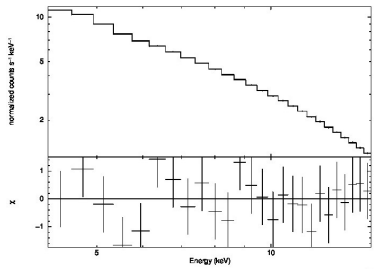

(g) Seventh phase spectrum

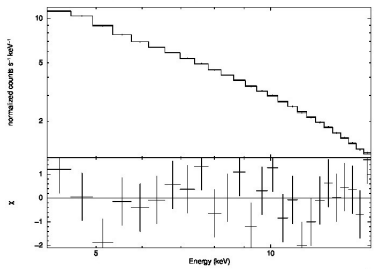

(h) Eighth phase spectrum

Figure A.5: Phase Spectra of XTE J1807-294 in First Flare State

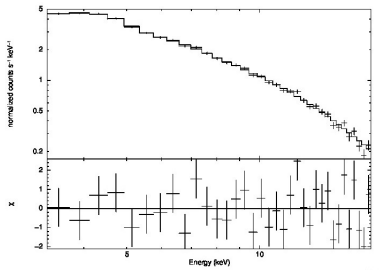

(a) First phase spectrum

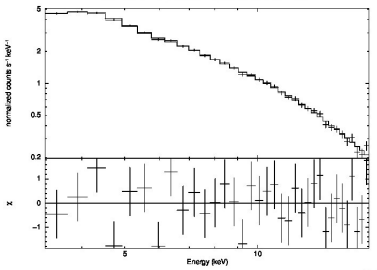

(b) Second phase spectrum

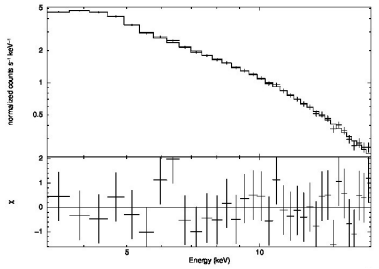

(c) Third phase spectrum

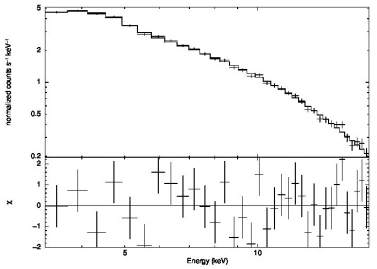

(d) Fourth phase spectrum

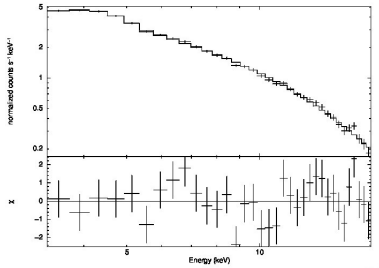

(e) Fifth phase spectrum

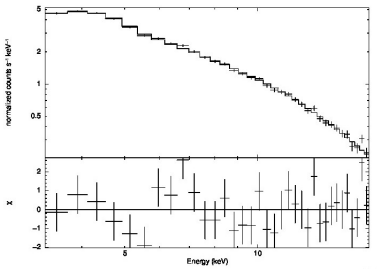

(f) Sixth phase spectrum

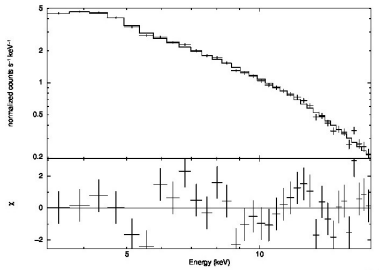

(g) Seventh phase spectrum

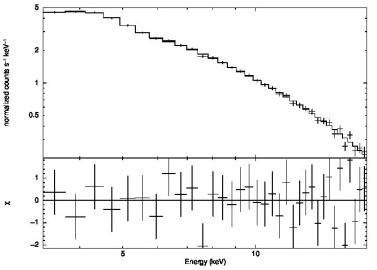

(h) Eighth phase spectrum

Figure A.6: Phase Spectra of XTE J1807-294 in Second Non-Flare State

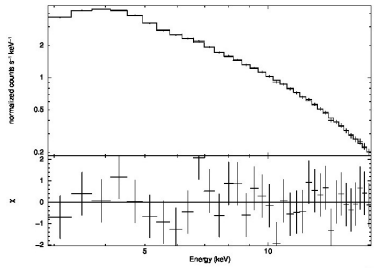

(a) First phase spectrum

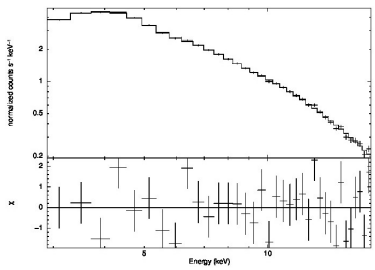

(b) Second phase spectrum

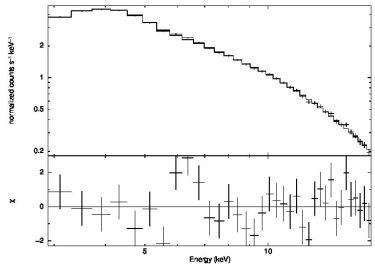

(c) Third phase spectrum

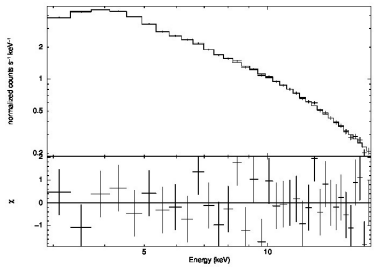

(d) Fourth phase spectrum

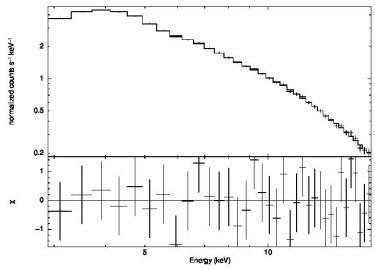

(e) Fifth phase spectrum

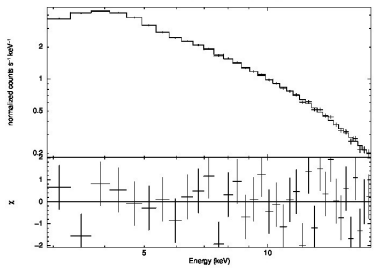

(f) Sixth phase spectrum

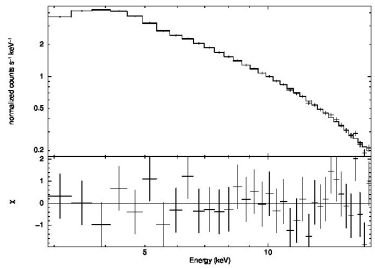

(g) Seventh phase spectrum

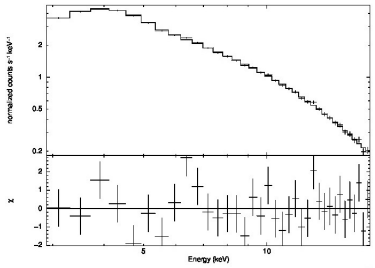

(h) Eighth phase spectrum

Figure A.7: Phase Spectra of XTE J1807-294 in Second Flare State

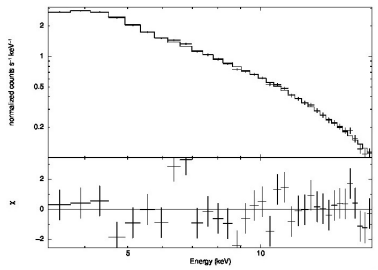

(a) First phase spectrum

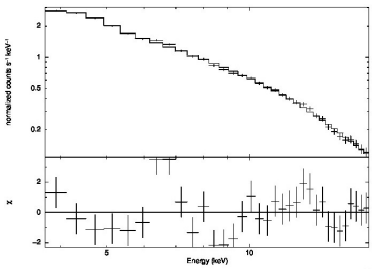

(b) Second phase spectrum

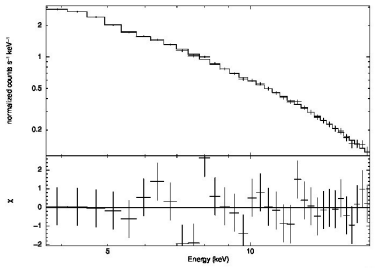

(c) Third phase spectrum

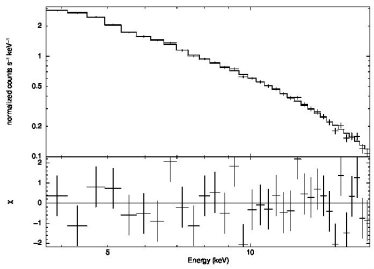

(d) Fourth phase spectrum

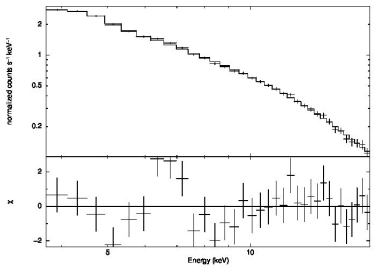

(e) Fifth phase spectrum

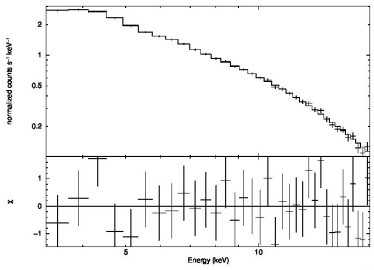

(f) Sixth phase spectrum

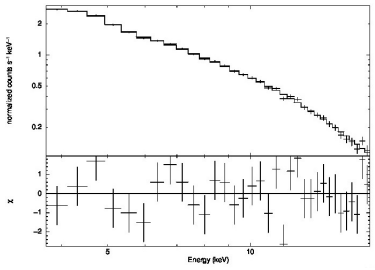

(g) Seventh phase spectrum

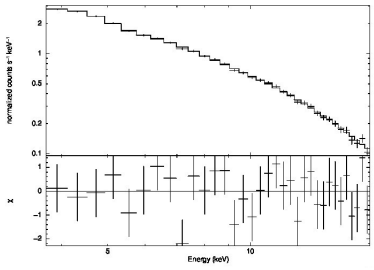

(h) Eighth phase spectrum

Figure A.8: Phase Spectra of XTE J1807-294 in Third Non-Flare State

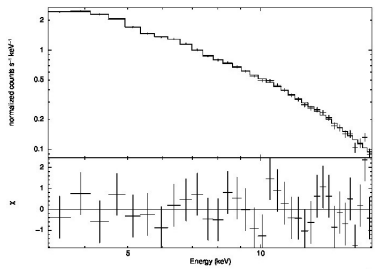

(a) First phase spectrum

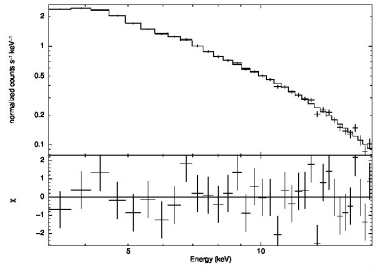

(b) Second phase spectrum

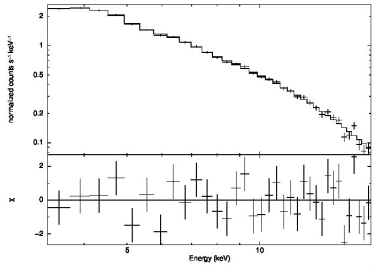

(c) Third phase spectrum

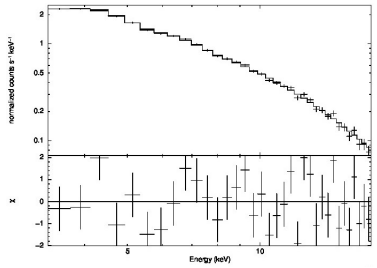

(d) Fourth phase spectrum

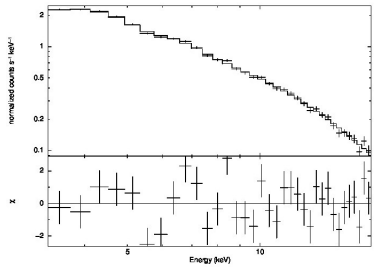

(e) Fifth phase spectrum

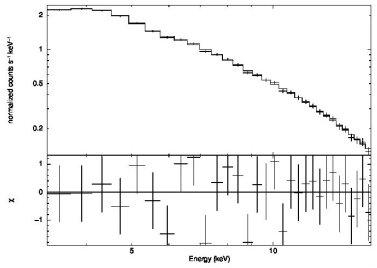

(f) Sixth phase spectrum

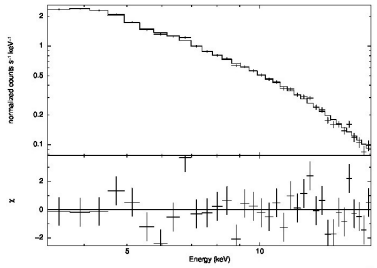

(g) Seventh phase spectrum

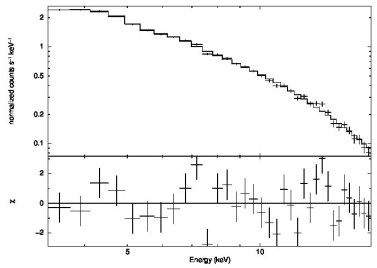

(h) Eighth phase spectrum

Figure A.9: Phase Spectra of XTE J1807-294 in Third Flare State

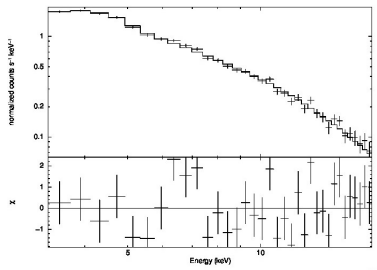

(a) First phase spectrum

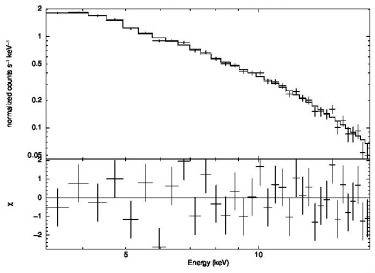

(b) Second phase spectrum

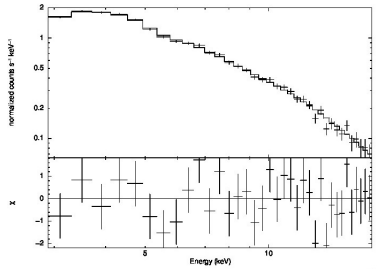

(c) Third phase spectrum

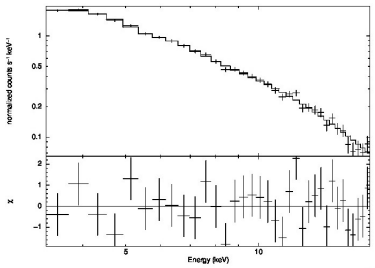

(d) Fourth phase spectrum

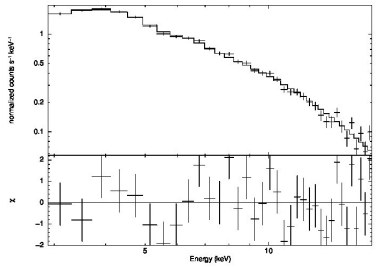

(e) Fifth phase spectrum

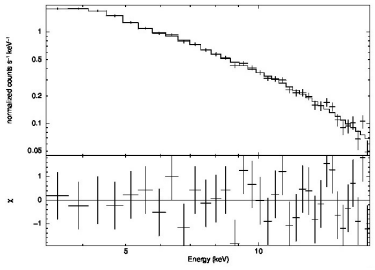

(f) Sixth phase spectrum

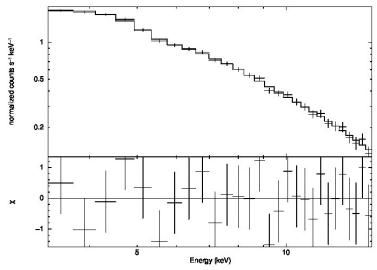

(g) Seventh phase spectrum

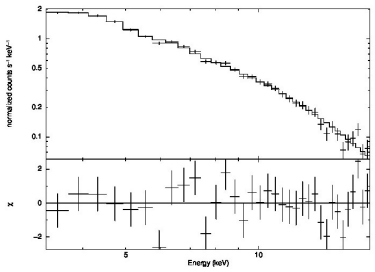

(h) Eighth phase spectrum

Figure A.10: Phase Spectra of XTE J1807-294 in Fourth Non-Flare State

APPENDIX B

Observation IDs of XTE J0929-314

Analysis of XTE J0929-314 in 2002 outburst cover 43 days of the outburst.

Table B.1: Observation IDs of XTE J0929-314

ObsID (70096)	Date	Exp. (s)	ObsID (70096)	Date	Exp. (s)
03-02-00	2002-05-09 10:36:54.7	2047	03-09-00	2002-05-24 06:53:55.7	1805
03-02-01	2002-05-09 12:16:26.7	2517	03-09-01	2002-05-25 08:09:32.5	3467
03-03-01	2002-05-11 06:48:48.1	3504	03-09-02	2002-05-26 05:00:44.6	4888
03-03-00	2002-05-11 10:04:47.1	7401	03-10-00	2002-05-27 04:32:30.3	2700
03-04-00	2002-05-12 09:48:44.6	3690	03-10-02	2002-05-27 21:58:01.9	1136
03-04-01	2002-05-13 09:32:42.1	3756	03-10-01	2002-05-27 23:32:30.6	1557
03-05-01	2002-05-13 15:52:52.6	11471	03-10-03	2002-05-28 23:22:31.9	1013
03-06-01	2002-05-14 12:35:16.8	2483	03-10-04	2002-05-29 01:02:28.9	1080
03-06-00	2002-05-14 14:15:12.1	18272	03-11-00	2002-05-29 22:57:44.9	1530
03-05-00	2002-05-15 11:11:01.5	5152	03-12-00	2002-05-31 02:01:56.4	1925
03-07-00	2002-05-15 13:53:57.7	13140	03-12-01	2002-06-01 09:37:17.8	1038
03-07-01	2002-05-16 13:35:56.8	14461	03-12-02	2002-06-03 23:23:51.4	1637
03-08-00	2002-05-17 10:07:31.3	957	03-12-03	2002-06-04 19:55:16.3	808
03-08-01	2002-05-17 13:24:33.4	711	03-12-05	2002-06-06 22:34:27.8	1563
03-08-02	2002-05-18 22:38:28.9	1622	03-13-00	2002-06-13 08:14:42.7	2611
03-08-03	2002-05-19 10:05:00.1	594	03-14-01	2002-06-16 04:33:45.5	1704
03-08-04	2002-05-20 07:53:06.7	643	03-14-00	2002-06-17 05:31:04.2	3048
03-08-05	2002-05-21 19:04:41.1	1471	03-14-02	2002-06-18 21:26:22	909
03-08-06	2002-05-22 12:11:32.9	888	03-14-03	2002-06-19 23:06:23.3	908
03-08-07	2002-05-23 18:16:33.6	768	03-14-04	2002-06-20 19:25:27.8	1380

Observation IDs of IGR J00291+5954

Analysis of IGR J00291+5954 in 2008 September outburst cover 11 days of outburst and consist of observed 8 days.

Table B.2: Observation IDs of IGR J00291+5954

ObsID (93013)	Date	Exp. (s)
07-17-00	2008-09-21 11:51:06.9	903
07-17-01	2008-09-23 09:10:20.4	1214
07-18-02	2008-09-24 08:11:35.2	885
07-18-00	2008-09-24 23:29:30.9	1071
07-17-02	2008-09-25 12:27:40.6	11188
07-20-01	2008-09-26 20:55:33	2509
07-19-00	2008-09-27 08:56:26.6	1142
07-20-03	2008-09-27 22:05:26.9	3780
07-19-01	2008-09-30 16:21:10.4	755
07-19-02	2008-09-30 19:07:10.6	2134
07-20-02	2008-09-30 20:48:10.7	1714
07-20-00	2008-10-01 02:12:07.2	713

Observation IDs of IGR J17498-2921

Observation IDs which are used for the analysis can be found below. Analysis of IGR J17498-2921 in 2011 outburst cover 39 days of the outburst.

Table B.3: Observation IDs of IGR J17498-2921

ObsID (96435)	Date	Exp. (s)	ObsID (96435)	Date	Exp. (s)
01-02-00	2011-08-15 20:21:27.1	5320	01-04-03	2011-08-29 08:39:06.3	3106
01-02-01	2011-08-16 12:00:09.5	15278	01-04-04	2011-08-30 16:03:45.8	3439
01-02-02	2011-08-17 16:13:47.1	3023	01-04-05	2011-08-31 09:12:38.6	2980
01-02-03	2011-08-18 12:28:03.1	6827	01-04-06	2011-09-01 08:43:34.2	3285
01-03-00	2011-08-19 07:26:06.7	37799	01-05-00	2011-09-02 05:05:11.6	2434
01-03-02	2011-08-19 18:23:06.7	3584	01-05-01	2011-09-03 07:39:21.6	2650
01-03-03	2011-08-19 21:28:38.5	3463	01-05-02	2011-09-04 11:58:56.9	3280
01-03-01	2011-08-20 09:58:37.3	21402	01-05-03	2011-09-05 05:05:53.1	2407
01-03-04	2011-08-21 12:42:07.2	7137	01-05-04	2011-09-06 03:04:22.7	1991
01-03-05	2011-08-22 12:12:56.7	3423	01-05-05	2011-09-07 02:31:56.1	1927
01-03-06	2011-08-23 14:51:06.9	6930	01-05-06	2011-09-08 05:45:06.6	1537
01-03-07	2011-08-24 09:37:59.2	3240	01-06-04	2011-09-14 05:41:36.7	1965
01-03-08	2011-08-25 12:18:32	3342	01-06-05	2011-09-15 11:24:18.1	2277
01-04-00	2011-08-26 17:59:48.8	3441	01-07-00	2011-09-20 12:00:08.6	1957
01-04-01	2011-08-27 17:34:14.3	3391	01-07-01	2011-09-22 09:24:18.4	2468
01-04-02	2011-08-28 07:37:19.8	2840			

Observation IDs of XTE J1807-294

Analysis of XTE J1807-294 in 2003 outburst cover 150 days of the outburst.

Table B.4: Observation IDs of XTE J1807-294

ObsID (80145)	Date	Exp. (s)	ObsID (80145)	Date	Exp. (s)
First non-flare state			Second non-flare state		
01-01-01	2003-02-28 12:55:16	2367	01-04-05	2003-03-19 17:58:22.4	2831
01-01-02	2003-02-28 23:50:28.9	2340	01-04-07	2003-03-19 21:08:17.7	3441
01-01-03	2003-03-01 12:35:30.6	2157	01-04-08	2003-03-20 20:50:07.3	7077
01-01-04	2003-03-01 14:18:36.9	2086	01-05-01	2003-03-21 00:03:06.6	6834
01-01-00	2003-03-01 23:32:28	10141	01-05-03	2003-03-21 22:06:46.4	3447
First flare state			Second flare state		
01-02-00	2003-03-04 22:45:01.2	7135	01-05-02	2003-03-22 00:03:22.2	2052
01-02-03	2003-03-06 15:55:25.5	1566	01-05-00	2003-03-22 17:02:59.4	4313
01-02-02	2003-03-06 17:34:25.5	1746	01-05-11	2003-03-22 19:16:07.1	1314
01-02-01	2003-03-06 19:12:25.9	8706	01-05-05	2003-03-23 16:43:58.1	6784
01-03-03	2003-03-07 12:21:16.1	1647	01-05-06	2003-03-25 00:34:06.8	2081
01-03-02	2003-03-07 21:50:16.2	7043	01-05-04	2003-03-25 17:39:56.4	3426
01-03-00	2003-03-08 23:38:28.3	8760	01-05-08	2003-03-26 23:59:55.7	2163
01-02-04	2003-03-10 00:21:14.4	17552	01-05-07	2003-03-27 15:52:42.2	1594
01-02-06	2003-03-11 00:02:12.2	17437	01-05-10	2003-03-27 17:27:10.9	2014
01-01-05	2003-03-12 01:21:26.8	6906	01-05-09	2003-03-27 18:36:00	3419
01-03-01	2003-03-12 20:18:06.6	11946	01-06-00	2003-03-28 16:45:07.2	6782
01-02-05	2003-03-13 18:23:35.2	12407	01-06-07	2003-03-29 11:56:06.7	1373
01-04-01	2003-03-14 00:00:06.9	3835	01-06-01	2003-03-29 14:45:26.5	3427
01-04-00	2003-03-14 21:10:07.4	10426	01-06-10	2003-03-29 17:55:19.2	3019
01-04-02	2003-03-16 00:04:57.2	6828	01-06-02	2003-03-30 14:30:39.2	6278
01-04-10	2003-03-16 03:46:07.4	1482	01-06-03	2003-03-31 11:43:39.4	11379
01-04-03	2003-03-16 20:36:06.6	10265	01-06-04	2003-04-01 18:36:57	6418
01-04-04	2003-03-17 18:41:07.6	2982			
01-04-09	2003-03-18 04:39:22.5	1330			
01-04-11	2003-03-18 23:06:57	6839			

Table B.5: Observation IDs of XTE J1807-294 (Cont.d)

ObsID (80145)	Date	Exp. (s)	ObsID (80145)	Date	Exp. (s)
	Third non-flare state			Fourth non-flare state	
01-06-05	2003-04-02 15:04:52.9	6910	01-13-02	2003-05-20 09:00:51.8	6373
01-06-08	2003-04-03 10:35:56.8	1379	01-13-03	2003-05-22 16:22:07.4	6015
01-06-09	2003-04-03 11:53:59.7	2276	01-14-00	2003-05-24 14:04:11.1	6811
01-06-06	2003-04-03 19:37:52.6	2953	01-14-01	2003-05-26 07:10:47.4	6503
01-07-04	2003-04-04 05:30:20.2	1456	01-14-02	2003-05-29 06:24:44.4	4227
01-07-00	2003-04-04 19:21:06.9	3050	01-15-00	2003-05-31 07:16:48.6	2723
01-07-03	2003-04-06 14:07:18.6	2181	01-15-03	2003-05-31 15:05:39.6	3151
01-07-02	2003-04-10 17:51:06.9	4807	01-15-02	2003-06-03 06:02:04.4	6467
01-08-00	2003-04-12 21:35:07.3	5809	01-16-00	2003-06-08 13:58:10	3461
01-08-01	2003-04-14 15:48:06.6	7320	01-16-02	2003-06-10 08:40:11.1	2016
01-08-02	2003-04-16 19:09:07.2	1497	01-16-03	2003-06-12 04:49:07.4	2151
01-08-03	2003-04-16 23:26:01.8	1441	01-17-00	2003-06-14 04:10:06.8	1912
01-08-04	2003-04-17 05:31:54.3	3851	01-17-01	2003-06-16 16:08:24	1451
01-09-00	2003-04-18 06:48:54.1	7628	01-17-02	2003-06-18 17:03:32.3	1494
01-09-01	2003-04-20 20:17:34.7	7311	01-18-00	2003-06-20 16:24:06.6	848
01-09-02	2003-04-22 21:25:56.9	3651	01-18-01	2003-06-22 17:20:00.7	1738
01-09-03	2003-04-24 16:04:07.4	6242			
01-10-00	2003-04-26 18:35:07.3	7071			
01-10-01	2003-04-28 14:43:58.4	5581			
	Third flare state				
01-10-02	2003-04-30 22:02:07.3	7007			
01-11-00	2003-05-02 18:13:07.1	6950			
01-11-01	2003-05-04 15:59:06.7	6470			
01-11-02	2003-05-06 16:50:04.4	6951			
01-11-03	2003-05-08 16:09:07.2	6825			
01-12-00	2003-05-10 14:01:07.1	6219			
01-12-01	2003-05-12 13:17:06.7	6885			
01-12-02	2003-05-14 12:38:07.9	6823			
01-13-00	2003-05-16 16:46:06.8	6870			
01-13-01	2003-05-18 11:13:23.2	6851			